JGR Solid Earth

RESEARCH ARTICLE
10.1029/2019JB017611

Key Points:
- Wide-angle seismic data show upper crustal velocity change at Higgins-Zietz boundary
- Rifting to form the South Georgia Basin localized south of the tectonic suture at the Higgins-Zietz boundary
- Recent earthquakes localize along the Higgins-Zietz orogenic and rift-related boundary

Supporting Information:
- Supporting Information S1
- Figure S1
- Table S1
- Table S2
- Data Set S1
- Data Set S2

Correspondence to:
R. E. Marzen,
rmarzen@ldeo.columbia.edu

Citation:
Marzen, R. E., Shillington, D. J., Lizarralde, D., & Harder, S. H. (2019). Constraints on Appalachian orogenesis and continental rifting in the southeastern United States from wide-angle seismic data. *Journal of Geophysical Research: Solid Earth*, *124*. https://doi.org/10.1029/2019JB017611

Received 27 FEB 2019
Accepted 12 JUN 2019
Accepted article online 24 JUN 2019

Constraints on Appalachian Orogenesis and Continental Rifting in the Southeastern United States From Wide-Angle Seismic Data

Rachel E. Marzen[1], Donna J. Shillington[1], Daniel Lizarralde[2], and Steven H. Harder[3]

[1]Lamont-Doherty Earth Observatory of Columbia University, Palisades, NY, USA, [2]Woods Hole Oceanographic Institution, Woods Hole, MA, USA, [3]Department of Geological Sciences, University of Texas at El Paso, El Paso, TX, USA

Abstract The Southeastern United States is an ideal location to understand the interactions between mountain building, rifting, and magmatism. Line 2 of the Suwannee suture and Georgia Rift basin refraction seismic experiment in eastern Georgia extends 420 km from the Inner Piedmont to the Georgia coast. We model crustal and upper mantle V_P and upper crustal V_S. The most dramatic model transition occurs at the Higgins-Zietz magnetic boundary, north of which we observe higher upper crustal V_P and V_S and lower V_P/V_S. These observations support the interpretation of the Higgins-Zietz boundary as the Alleghanian suture. North of this boundary, we observe a low-velocity zone less than 2 km thick at ~5-km depth, consistent with a layer of sheared metasedimentary rocks that forms the Appalachian detachment. To the southeast, we interpret synrift sediments and decreasing crustal thickness to represent crustal thinning associated with the South Georgia Rift Basin and subsequent continental breakup. The correspondence of the northern limit of thinning with the interpreted suture location suggests that the orogenic suture zone and/or the Gondwanan crust to the south of the suture helped localize subsequent extension. Lower crustal V_P and V_P/V_S preclude volumetrically significant mafic magmatic addition during rifting or associated with the Central Atlantic Magmatic Province. Structures formed during orogenesis and/or extension appear to influence seismicity in Georgia today; earthquakes localize along a steeply dipping zone that coincides with the northern edge of the South Georgia Basin and the change in upper crustal velocities at the Higgins-Zietz boundary.

1. Introduction

Many questions remain about the style of orogenesis in ancient orogens and the effects of orogenic structures on later tectonic events. The style of orogenic deformation is influenced by the amount of total shortening, the degree of obliquity of collision, rheological contrasts between terranes, and properties of preexisting weak zones such as sedimentary layers from continental margins (e.g., Pfiffner, 2017). For example, mechanically weak, anisotropic, and/or low-velocity detachment layers have been identified in regions with large amounts of orthogonal collision such as the Himalayas (Schulte-Pelkum et al., 2005) and the central Andes (Yuan et al., 2000), and steeply dipping structures are thought to form in regions with significant transpression (e.g., Kashubin & Juhlin, 2010; Schreurs & Colleta, 1998; Teyssier et al., 1995; Wilson et al., 2004). Identifying and characterizing structures in ancient orogens can enable improved reconstructions of their histories; however, this often proves difficult. The southern Appalachians are one of the best-known ancient orogens, yet the locations, ages, and geometries of major sutures and the resulting lithospheric configuration remain controversial.

The lithospheric configuration created by orogenesis, including crustal faults and shear zones, can also influence later tectonic events, such as continental rifting. Inherited crustal weaknesses can come in the form of thermal, compositional, or structural features that preferentially accommodate deformation if favorably oriented (e.g., Beaumont & Ings, 2012; Chenin et al., 2015; Dunbar & Sawyer, 1989; Gernigon et al., 2014; Keranen & Klemperer, 2008; Manatschal et al., 2015; Seranne et al., 1995; Thomas, 2006; Tommasi & Vauchez, 2001). Recent examinations of structural inheritance in eastern North America and other ancient and active rifts suggest that preexisting structures may be particularly important in localizing extension during the early phases of continental rifting (Manatschal et al., 2015). Analyzing the role of preexisting orogenic structures on subsequent rifting requires high-quality data that constrain the geometry, properties, and role of inherited structures in individual orogenic systems. Finally, structures formed during past

orogenesis and rifting may control present-day intraplate deformation (Pratt et al., 2015), so better constraints on crustal structures can improve our understanding of modern seismicity.

This study focuses on the southeastern United States to examine the relationship between preexisting orogenic structures, rifting, and magmatism. Because this region was central to the building of the Appalachian orogen, extension to form rift basins along the eastern margin including the South Georgia Basin, emplacement of the large Central Atlantic Magmatic Province (CAMP), and finally breakup of Pangea and opening of the Atlantic Ocean, it is an ideal location for this study. In this paper, constraints on V_P and V_S from a seismic refraction profile in eastern Georgia are used to constrain lithologic properties of the crust including accreted terranes, the locations and geometries of suture zones between terranes, and the role of orogenic structures on subsequent rifting, magmatism, and modern seismicity.

2. Tectonic Background

The Appalachian orogen was built during the Ordovician-Silurian Taconic orogeny, the Devonian Acadian and Devonian-Mississippian Neoacadian orogenies, and the Pennsylvanian-Permian Alleghanian orogeny (e.g., Hatcher et al., 2007; Hibbard et al., 2012). The first two orogenies were terrane accretion events, while the final orogeny resulted in the closure of the Iapetus Ocean and formation of the Pangea supercontinent. After the amalgamation of Pangea, extension beginning in the late Triassic (~230 Ma) formed a series of basins, including the South Georgia Rift basin (e.g., Withjack et al., 2012). Extension associated with basins in the southern segment of the Eastern North American Margin may have ceased by ~205 Ma (Withjack et al., 2012) and was followed by extensive magmatism from the CAMP at ~201 Ma (Blackburn et al., 2013; Marzoli, 1999) and the successful breakup of Pangea afterward. Because the southeastern United States was central to these mountain-building, rifting, and magmatic events, its crustal structure records the interactions between these processes.

2.1. Paleozoic Orogenic Events and Terrane Accretion

Here we focus on the expression of orogenic events in the southernmost Appalachians. The terranes covered by our study are the Inner Piedmont, Carolina, Charleston/Brunswick, and Suwannee terranes (Figure 1). To the north of the sediment-covered coastal plain, the boundaries between accreted terranes at the surface have been identified based on abrupt contrasts in stratigraphy, metamorphic histories, composition, and tectonic structures (e.g., Williams & Hatcher, 1982); the Inner Piedmont, Carolina, and small parts of the Charleston/Brunswick terrane lie north of the coastal plain, while the southern part of the Charleston/Brunswick terrane and the Suwannee terrane lie beneath the coastal plain.

The Inner Piedmont consists primarily of metasedimentary rocks thought to have been deposited on oceanic crust outboard of the Laurentian margin and developed into an accretionary prism ahead of the Carolina Superterrane (Huebner et al., 2017; Merschat & Hatcher, 2007). The region can be divided into a western portion of Laurentian affinity rocks and an eastern portion of Laurentian and Peri-Gondwanan affinity rocks that accreted onto Laurentia during the Neoacadian orogeny (Huebner et al., 2017; Merschat & Hatcher, 2007). The Inner Piedmont is distinguished from the surrounding terranes by the relatively high metamorphic grade of its core (sillimanite I and II grade metamorphic rocks; Huebner et al., 2017) and is separated from neighboring terranes by highly sheared belts of lower grade rocks (Griffin, 1971).

To the southeast, the peri-Gondwanan Carolina Superterrane comprises multiple subterranes including a primitive island arc sequence that amalgamated before accreting onto the Laurentian margin (Hatcher et al., 2007; Whitney et al., 1978) and is largely composed of rocks of amphibolite and greenschist facies (Secor et al., 1986; Shervais et al., 2003). The timing and nature of accretion of the Carolina Terrane is debated (e.g., Hibbard, 2000) but may have occurred during the Neoacadian orogeny in a transpressional regime along the Central Piedmont Suture, which separates the Carolina Terrane from the Inner Piedmont (Hatcher et al., 2007). In the southeastern United States, field mapping along the Central Piedmont Suture reveals a strong strike-slip component of motion from the reactivation of these faults during the subsequent Alleghanian orogeny (Hatcher et al., 2007; Hooper et al., 1997; West, 1998). The Inner Piedmont may have been migmatized by subduction beneath the Carolina Terrane when the Carolina Terrane accreted onto Laurentia, and then erosion exposed the highly metamorphosed Inner Piedmont (Hatcher et al., 2007; Hatcher & Merschat, 2006). Perhaps in contrast to geological evidence for

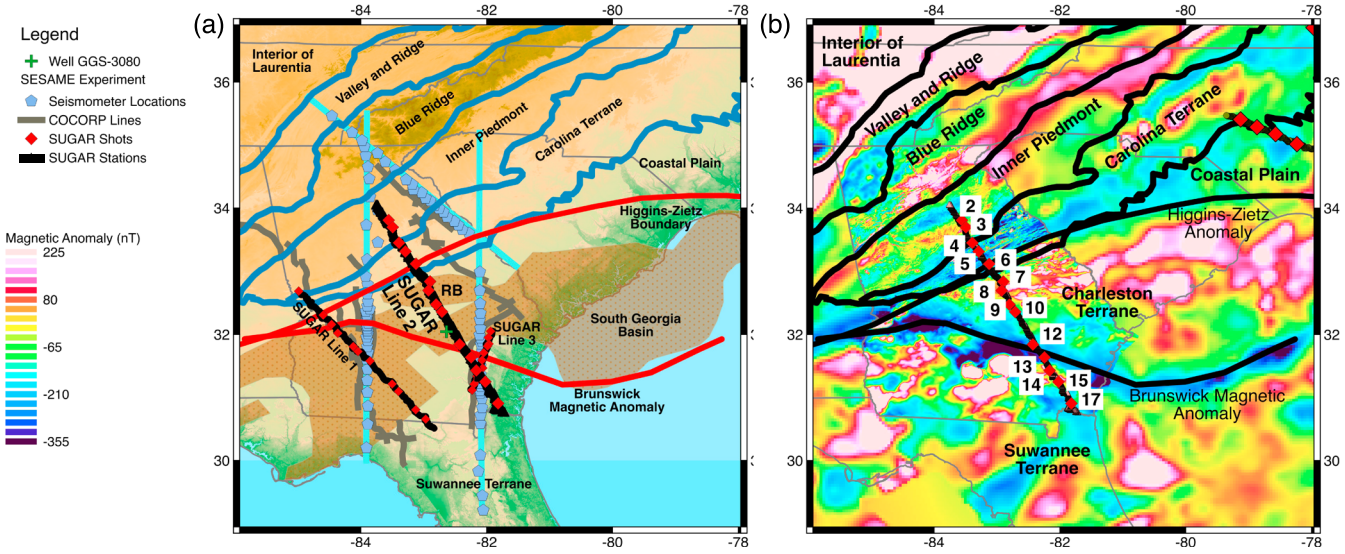

Figure 1. (a) Map of the SUGAR seismic lines in the southeastern United States. Outlines are drawn of simplified geological terrane boundaries (Hatcher et al., 2007; Steltenpohl et al., 2008), the outline of the South Georgia Basin (McBride et al., 1989), COCORP reflection seismic lines (e.g., Cook & Vasudevan, 2006; Nelson, Arnow, et al., 1985), SESAME broadband seismometer locations (e.g., Hopper et al., 2017; Parker et al., 2015), and the extent of the resulting receiver function CCP stack cross sections as underlying bright blue lines (Hopper et al., 2017). RB = Riddleville Basin. (b) Map of magnetic anomaly data (high-resolution data set inside Georgia, Daniels, 2001, and World Digital Magnetic Anomaly Map outside Georgia, Maus et al., 2007). Line 2 shots are numbered. SUGAR = SUwannee suture and GeorgiA Rift basin; COCORConsortium for Continental Reflection Profiling; SESAME = Southeastern Suture of the Appalachian Margin Experiment.

transpression during the Alleghanian orogeny, COCORP (Consortium for Continental Reflection Profiling) reflection seismic images show a shallow reflective detachment at ~2- to 4-s two-way traveltime (TWTT) that implies thin-skinned tectonic accretion of the Inner Piedmont and Carolina terranes (Cook et al., 1979; Cook & Vasudevan, 2006).

Farther south, the origin, extent, and nature of terranes and boundaries between them are more uncertain because they are mostly covered by coastal plain sediments. The Brunswick/Charleston terrane, another peri-Gondwanan terrane, has been proposed to lie south of the Carolina terrane based on limited drill site and magnetic data (Hatcher et al., 2007; Higgins & Zietz, 1983; Horton et al., 1989; Williams & Hatcher, 1982). Although our knowledge of the lithology of the Brunswick/Charleston terrane is limited, available rock samples suggest that the terrane is composed of greenschist facies rocks of sedimentary and volcanic origin (Horton et al., 1989). Finally, the Suwannee terrane is interpreted to lie farther south beneath southern Georgia and Florida, and it comprises Paleozoic sediments, granites, and felsic volcanic rocks thought to be derived from the African continent. A boundary of particular interest for this study is the Alleghenian suture that separates pre-Alleghanian Laurentia from the Brunswick/Charleston and Suwannee terranes that accreted onto Laurentia during the final orogeny that built the Appalachians—the Alleghanian orogeny (320–260 Ma).

The surface location of the suture between pre-Alleghanian Laurentia and the Brunswick and Suwannee terranes and the geometry of this suture at depth remain a subject of debate. The change in magnetic character (Figure 1b) and observation of a southward dipping band of reflections (~40°) throughout the crust in COCORP data (McBride, 1991; Nelson, Arnow, et al., 1985) supported the interpretation of the Brunswick Magnetic Anomaly (BMA) as the Alleghenian suture (Figure 1). However, drilling data suggest Gondwanan-affinity material lies north of this magnetic anomaly (Chowns & Williams, 1983), leading to the suggestion that the Higgins-Zietz magnetic boundary, which coincides with the Carolina-Mississippi fault, may mark the Alleghenian suture (Higgins & Zietz, 1983; Figure 1). Recent receiver-function imaging of a dipping midcrustal feature that shallows at the Higgins-Zietz magnetic boundary (Hopper et al., 2017) and the geographic extent of relatively undeformed Suwannee Basin sediments that predate the Alleghenian orogeny (Boote & Knapp, 2016) provide evidence that the Higgins-Zietz boundary marks the Alleghenian suture.

Recent findings that indicate that the Alleghanian suture lies north of the BMA raise questions about the origin and tectonic significance of the BMA itself. If the BMA is the boundary between the peri-Gondwanan Charleston terrane and the Gondwanan Suwannee terrane (Horton et al., 1989), the distribution of undeformed Paleozoic sediments (Boote & Knapp, 2016) suggests these two terranes docked onto Laurentia together after the deposition of the Suwannee Basin sediments. In summary, many questions remain about the nature and existence of terrane boundaries beneath the coastal plain, including (1) the location of the Alleghanian suture, (2) the extent and affinity of terranes beneath the coastal plain, and (3) the tectonic significance of the BMA. We seek to shed light on these questions with new constraints on crustal structure from the SUGAR (SUwannee suture and GeorgiA Rift basin) experiment.

2.2. Mesozoic Extension and CAMP Magmatism

Collision to form Pangea was followed by widespread extension as early as the Middle Triassic. The timing of rifting along the eastern North American margin is constrained by the ages of growth strata in rift basins, which indicate earliest extension in the southeastern United States and progressively younger extension to the north (Withjack et al., 2012). The South Georgia Basin is among the oldest of these rift basins, with extension occurring from ~230 to 205 (Withjack et al., 2012).

The current understanding of the distribution of synrift sediment deposition and crustal thinning is limited by available drill and seismic reflection data. COCORP reflection seismic data and well data show that the South Georgia Basin is a composite of asymmetric minibasins that may be up to 9 km thick, but sediment thickness is poorly constrained because of the paucity of velocity constraints on the basin sediments (Chowns & Williams, 1983; McBride et al., 1987). Crustal thickness measurements come from passive source seismic imaging (Parker et al., 2013; Schmandt et al., 2015) and can be inferred from Moho reflections in COCORP reflection seismic profiles, but the former are of lower resolution than active-source seismic constraints, and the latter require assumptions regarding crustal velocity structure.

The association of rift basins in eastern North America with Paleozoic collisional structures has been interpreted as collisional structures influencing the formation of some rift basins (e.g., Schlische, 2003; Withjack et al., 2012). However, in detail, this relationship is not always simple. For example, COCORP seismic reflection data suggest that the South Georgia Basin lies south of the Alleghenian suture in western Georgia (McBride, 1991) and that the rift basins are sometimes bound by north dipping border faults, in contrast to the southward dipping interpreted sutures (Nelson, Arnow, et al., 1985).

Following the onset of extension, the laterally extensive CAMP was emplaced over a large region including eastern North America, eastern South America, western Africa, and parts of Europe at ~201 Ma (Blackburn et al., 2013; Hames et al., 2000; Marzoli, 1999). U-Pb dating of and stratigraphy surrounding CAMP volcanic rocks suggest emplacement occurred over this large area over a time span of less than a million years (Blackburn et al., 2013; Olsen et al., 2003). Several origins have been proposed for CAMP, including thermal insulation beneath a super continent (Coltice et al., 2007), edge-driven convection (Deckart et al., 2005; King & Anderson, 1998; McHone, 2000), lithospheric delamination, and mantle upwelling (Callegaro et al., 2013; Whalen et al., 2015), or a mantle plume (Janney & Castillo, 2001; Oyarzun et al., 1997; Wilson, 1997).

Very few constraints exist on the distribution and volume of CAMP magmatic intrusions within the crust. Consequently, estimates of the total volume of CAMP are based primarily on shallow intrusives (e.g., McHone, 2003). Bright reflections associated with interpreted sutures in seismic reflection data have been interpreted to indicate that sutures may control the emplacement of CAMP magmatism in the crust (Barnes & Reston, 1992; McBride & Nelson, 1988), but the absence of information on deep crustal intrusions also leaves many questions on the influence of orogenic structures and extension on the intrusion of CAMP magmas.

Finally, extension farther east ultimately culminated in the breakup of Pangea and seafloor spreading offshore. The timing of offshore extension is not known, but links between onshore boreholes, offshore stratigraphy, and magnetic anomalies suggest that it followed CAMP (Klitgord & Schouten, 1986; Oh et al., 1991). Like rift basins onshore, offshore extension is thought to have been influenced by orogenic sutures and other preexisting structures (e.g., Nelson, McBride, et al., 1985; Tommasi & Vauchez, 2001).

By integrating new and existing constraints on suture zone locations and geometry, crustal thickness, and sediment thickness across the South Georgia Basin, we can provide additional constraints on the location

and character of collisional structures, the amount of extension that occurred, and the extent to which preexisting weak zones from the Appalachian orogeny controlled the distribution of rifting.

2.3. Modern Seismicity

Lastly, despite the fact that the eastern United States is a passive margin, the east coast is seismically active today (e.g., Chapman et al., 2016; Sykes et al., 2008; Wu et al., 2015). Seismicity in the eastern U.S. passive margin results from the balance of ridge push forces, glacial-isostatic adjustment, local stress field perturbations, and dynamic mantle processes (Ghosh et al., 2019), which can then reactivate favorably oriented preexisting weak zones in the crust (Zoback, 1992). The infrequent occurrence of large earthquakes such as the 1886 Charleston, SC, earthquake and the 2011 Mineral, VA, earthquake, however, illustrates the importance of characterizing the regional seismic hazard. In contrast to regions where dense seismic instrumentation and frequent seismicity make it possible to delineate active fault structures, the knowledge of such structures and their spatial extent is limited in the eastern United States. The role of ancient orogenic or rifting structures in recent intraplate earthquakes is controversial. In some cases, seismicity appears to reactivate old structures like the Appalachian detachment (Seeber & Armbruster, 1981), but in others, a combination of newly formed faults and preexisting faults may be involved (e.g., in the Mineral earthquake, Pratt et al., 2015) or seismicity only weakly correlates to well-known ancient structures (Sykes et al., 2008; Wagner et al., 2018). Further, because faults within continents tend to be loaded slowly by far-field tectonic forces, seismicity within continents is highly sensitive to surface processes and stress transfers from other faults. An important implication of this behavior is that seismicity within continents is best understood by modeling the intracontinental faults as a complex system and not as individual structures with characteristic earthquake recurrence intervals (Liu & Stein, 2016). By better characterizing the geometries of structures formed during Appalachian orogenesis and rifting with respect to modern seismicity, we can better characterize the preexisting weak zones in the crust of the southeastern United States and evaluate the degree to which modern seismicity is controlled by those structures.

2.4. Existing Geophysical and Geological Data

Several geophysical data sets (Figure 1) and geological observations from Georgia and the broader southeastern United States constrain properties of the crustal structure that complement crustal velocity measurements from the SUGAR refraction seismic experiment. COCORP reflection seismic lines image basin structure and reflectivity in the crust and of the Moho (e.g., Cook & Vasudevan, 2006; McBride, 1991; Nelson, Arnow, et al., 1985). They also image several prominent structures thought to form during orogenesis, including the bright, gently dipping Appalachian decollement beneath the Inner Piedmont and Carolina terranes and a zone of steeply dipping reflectivity interpreted as the Alleghenian suture. At broader length scales, receiver functions from the Southeastern Suture of the Appalachian Margin Experiment (SESAME) broadband seismic data provide constraints on V_S in the upper crust (Parker et al., 2015) and on the geometry of interfaces where velocity increases or decreases with depth in the 1- to 33-s period band (Hopper et al., 2017). Data from SESAME instruments were combined with data from the U.S. Transportable Array to image Earth structure over a broader region (Figure 1a). Recordings of wide-angle arrivals in the southern Appalachians from mine blasts provide spatially averaged V_P/V_S for the upper crust and whole crust (Hawman et al., 2012). Finally, larger-scale investigations of crustal structure and Moho depth from the EarthScope transportable array provide regional backbone constraints (e.g., Schmandt et al., 2015).

Published investigations of the surface geology (e.g., Griffin, 1971; Hibbard et al., 2002; Shervais et al., 2003; Whitney et al., 1978) and drilling data (Chowns & Williams, 1983) provide insight into the composition of accreted terranes, their boundaries at the surface, the approximate spatial extent of synrift basins, and point samples of their shallow velocity structure. Sonic log data from one of these wells (green cross in Figure 1) were used to constrain shallow sediment velocity structure down to 1 km (Chowns & Williams, 1983; J. Knapp, personal communication, Apr. 24, 2017). We integrate our new velocity models with these existing geophysical and geological constraints.

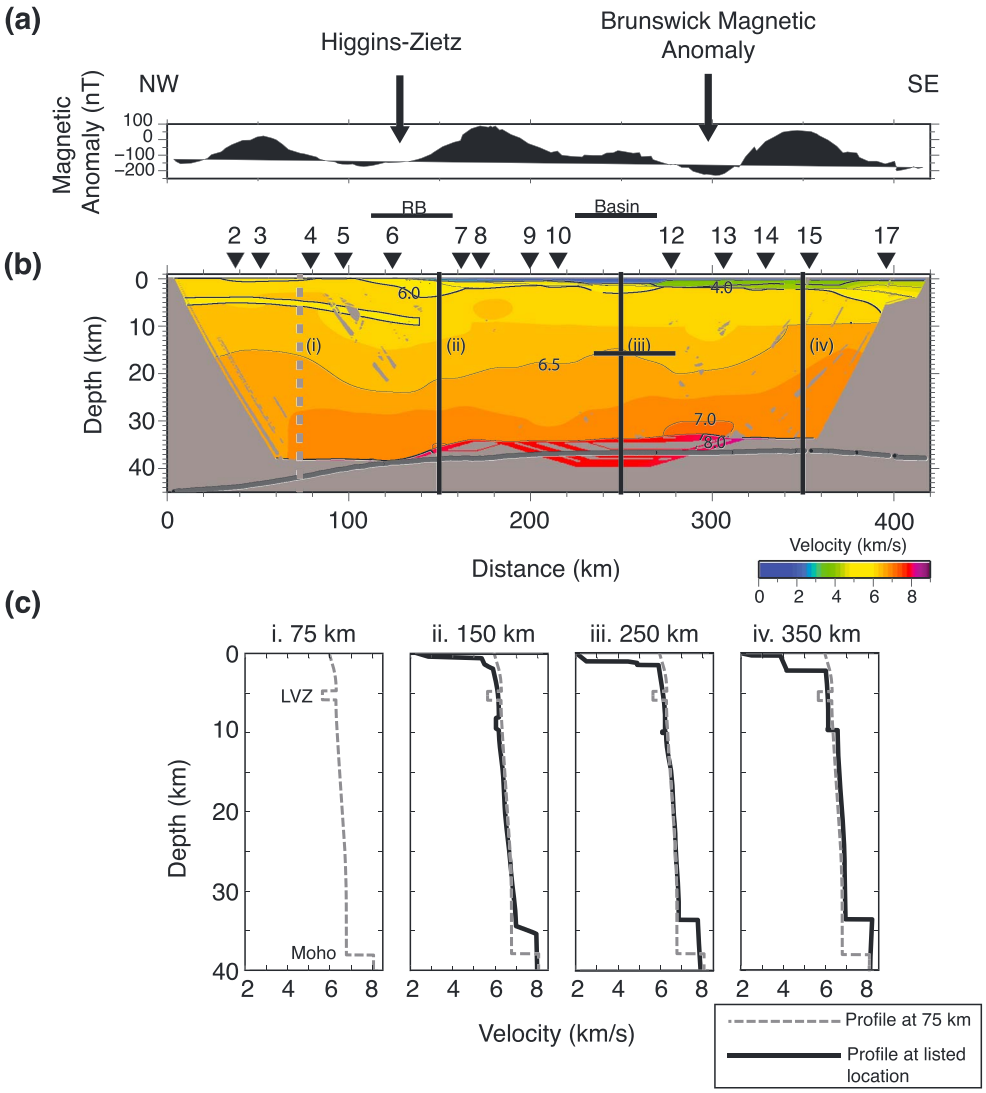

Figure 2. (a) Magnetic anomaly data (Maus et al., 2007) along the SUwannee suture and GeorgiA Rift basin seismic line highlighting the Higgins-Zietz boundary and Brunswick Magnetic Anomaly. (b) Inversion result for *P* wave velocity structure masked to show parts of the model constrained by ray coverage. Moho picks from (Schmandt et al., 2015) are overlain on the model for comparison. Shot locations are listed at triangles above the model. Lines and labels above model indicate two Mesozoic rift basins: the Riddleville Basin (RB) and another south Georgia subbasin (Basin). (c) Four 1-D velocity profiles taken at 75, 160, 250, and 350 km. The profile at 75 km is plotted as a dashed gray line behind other 1-D velocity profiles for comparison. LVZ = low-velocity zone.

3. Refraction Seismic Data Set Acquisition and Analysis

3.1. Data Acquisition

The SUGAR project involved the acquisition of wide-angle seismic reflection/refraction data on three transects designed to cross several major features, including (1) the previously inferred extent of the South Georgia Basin (McBride et al., 1989), (2) the Higgins-Zietz boundary (Higgins & Zietz, 1983) and BMA (e.g., Nelson, Arnow, et al., 1985; Pickering et al., 1977; Figure 2a), both of which have been proposed as potential suture zones between terranes (Boote & Knapp, 2016; Chowns & Williams, 1983; Hopper et al., 2017; Lizarralde et al., 1994; Tauvers & Muehlberger, 1987).

SUGAR Line 2 is a 420-km line of 1981 receivers at a nominal spacing of ~250 m that recorded 14 shots spaced at 20–50 km. The data were collected in August 2015. The map in Figure 1 shows the locations of shots and instruments for Lines 1, 2, and 3. The map also shows the locations of nearby reflection lines

Table 1
Shot Information

Shot number	Time (YYYY:JDD:hr:mn:ss.sss)	Latitude	Longitude	Charge size (kg)
202	2015:219:03:20:00.020	33.80847	−83.55728	273
203	2015:219:07:20:00.020	33.69766	−83.49372	182
204	2015:219:05:50:00.020	33.45043	−83.39242	727
205	2015:219:08:51:00.020	33.31253	−83.29161	182
206	2015:220:03:00:00.020	33.11601	−83.12384	182
207	2015:220:04:10:00.020	32.83597	−82.89922	182
208	2015:220:05:10:00.020	32.69918	−82.92459	182
209	2015:220:06:18:00.020	32.47656	−82.80255	364
210	2015:220:05:05:00.020	32.35993	−82.71048	182
212	2015:220:03:05:00.020	31.84319	−82.42969	182
213	2015:219:09:16:00.020	31.63764	−82.24596	182
214	2015:219:08:06:00.020	31.43025	−82.16371	182
215	2015:219:06:35:00.020	31.25057	−82.02168	182
217	2015:219:03:15:00.020	30.90663	−81.81776	727

from COCORP and broadband seismometers from SESAME, which provide complementary constraints on the structure of the crust.

IRIS PASSCAL provided the 1981 RefTek 125A dataloggers and Geospace GS11D 4.5-Hz geophones that recorded the seismic shots. Shot holes were 30.5 cm (12 in.) in diameter and cartridges 25.4 cm (10 in.) in diameter. The shots comprised cartridges filled with bulk emulsion blasting agent and primed with pentolite boosters. Shots were buried between 12 and 25 m beneath the surface, and the remainder of the shot hole was filled with gravel, drill cuttings, and bentonite. Shot locations, times, and charge sizes are listed in Table 1. Sixteen teams of students deployed the geophones and dataloggers on 4–6 August, which recorded shots detonated at night on August 6 and 7. The teams then recovered the geophones and dataloggers on 8–9 August.

Because the geophones were deployed along roads but the shots were placed off the road in locations far from any structures for safety, there is some three-dimensionality to the geometry of shots and recording geophones on SUGAR Line 2 (Figure 1). This three-dimensionality was especially large at near offsets between shots and receivers when the shots were located a few kilometers from the 2-D line.

3.2. Seismic Data Processing and Phase Identification

We applied basic signal processing techniques before picking arrivals, including bandpass filtering with cut-off frequencies of 3–14 Hz (*P* waves) and 0–8 Hz (*S* waves), weighting of traces by offset, applying appropriate reduction velocities for the phases being analyzed, trace mixing, and gain control (Cohen & Stockwell, 2002).

In portions of the line with significant sedimentary layers, we observed *P* wave sedimentary refractions out to ~15-km offset. Crustal refractions (*Pg*) are identified as first and secondary arrivals out to offsets up to 250 km, and we observe mantle refractions (*Pn*) on multiple shots, where the crossover distance of *Pg* and *Pn* decreases from a source-receiver offset of ~180 km in the north to ~160 km in the south. *PmP* arrivals were typically identified at offsets between 80 and 180 km. We picked *P* wave arrivals on all 14 shots including refractions through the sediments, crust, and mantle, and reflections off the Moho. We also observed mid-crustal reflections but did not use them to constrain the velocity models because (1) they were difficult to correlate between shots, making their potentially steeply dipping geometry uncertain, and (2) did not appear to be associated with a slope change in crustal refractions and are therefore unlikely to be associated with a significant contrast in crustal velocity.

In addition to *P* wave arrival picks, we also identified *S* wave crustal refractions and often Moho reflections in the northernmost 10 shots. In the northern shots 2–4, we only observed *Sg* arrivals to offsets <100 km but observed clear arrivals on shots 5–12 near the center of the line out to offsets of 140 km. We observed *SmS* reflections at offsets of ~80–140 km, which provide constraints on average V_S of the crust.

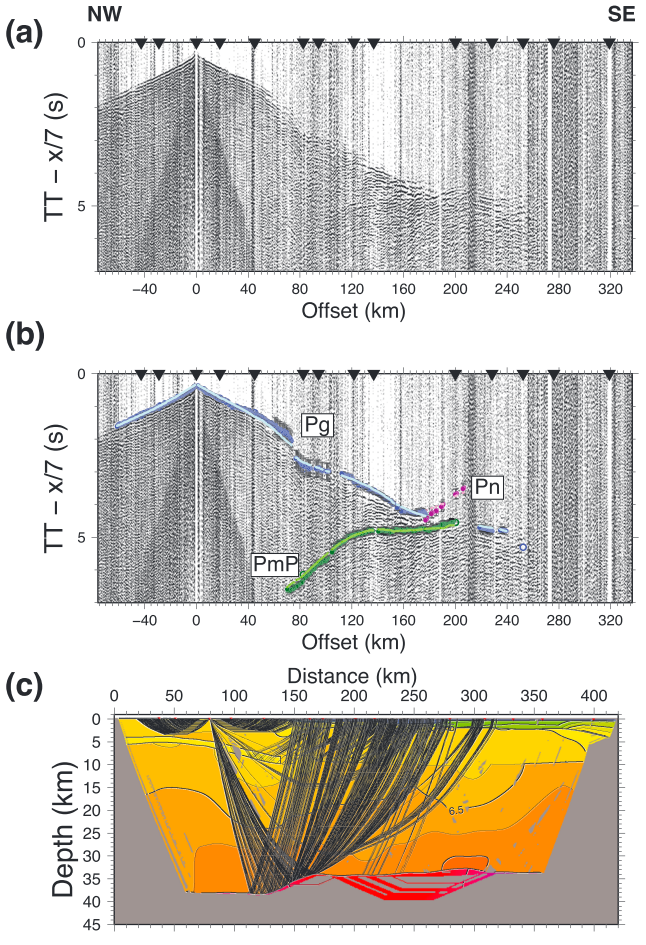

Figure 3. (a) Uninterpreted and (b) interpreted seismic data with *P* wave traveltime picks (dark color with error bars) and model calculated picks (pale color) from Shot 4 reduced at 7 km/s. Triangles above the *x* axes show the locations of other shots, and circles show reciprocity checks from picks on other shots. (c) Raypaths of the picked arrivals through the velocity model.

P wave and *S* wave arrival phase identifications were cross-checked for consistency against picks from other shots by comparing reciprocal picks (open circles in Figures 3–5). The reciprocity checks verify that traveltime from point A to point B is the same as from point B to point A, where A is the shot location and B is the receiver location. We also undertook forward modeling and inversion using RAYINVR (Zelt & Smith, 1992) to test phase identifications. Phase arrival picking was an iterative process where reciprocity checks from the highest signal-to-noise ratio shots helped constrain phase identifications on shots where the signal-to-noise ratio was lower. Error bars were visually assigned to picks including consideration for the alignment of reciprocity checks and ranged from 0.04 to 0.25 s, with smaller errors typically assigned at nearer source-receiver offsets (Tables 2 and 3). Larger errors were also assigned where significant topography in *Pg* arrivals was associated with abrupt changes in basin thickness to account for the slight three-dimensionality of the source receiver geometry and to limit the extent to which an imperfect basin model modified upper crust velocities.

Figures 3–5 show data from Shots 4, 8, and 17, respectively. Data from Shot 4 is characteristic of shots north of the coastal plain, where we observe (1) an absence of sedimentary refractions and (2) relatively high apparent velocities (~6.3 km/s) of arrivals at short source-receiver offsets reflecting relatively high upper-crustal velocities that are (3) followed by ~0.5 s delay in arrivals. This traveltime delay, which appears at ~80-km offset on northern shots, cannot be modeled as a thickness change of low-velocity sedimentary material at the Earth's surface and therefore provides evidence for a low-velocity zone (LVZ) in the shallow crust. This traveltime delay is also observed in the data for Shot 8 in *Pg* arrivals at negative offsets, which sample crust in the northern portion of Line 2. Figure 5 shows data from Shot 17 with features more typical to shots from the southern half of the line, including (1) refractions through slow sediments that were used to constrain basin structure, (2) slower apparent velocities for *Pg* arrivals at near offsets compared with shots farther north, and (3) no shadow zone associated with an upper crustal LVZ.

Figures 6 and 7 show data examples from Shots 4 and 9 reduced at 4.0 km/s with picks on refractions through the upper crust. Although there is greater uncertainty in the *S* wave arrivals, there are many similarities between the *S* wave and the *P* wave data. We do not observe refractions through the sediment in the *S* wave data, but the traveltime delay to the first crustal refractions is greater where we observe greater sediment thickness in the *P* wave data. In the north, the apparent velocity of the crustal refractions implies relatively high upper crust *S* wave velocities ~3.9 km/s followed by a traveltime delay at ~50-km offset that is consistent with the LVZ we observe in the *P* wave arrivals. Although a delay can be observed, it is not possible to confidently pick refractions after the shadow zone, so we do not model it here.

The supporting information shows the remaining shot data and arrival picks that we used to invert for velocity structure. In sections 3.3–3.5 below, we describe how these arrivals were used to constrain inversions for the *P* wave, *S* wave, and V_P/V_S structure of the sediments, crust, and upper mantle along SUGAR Line 2.

3.3. Experiment Geometry and Model Setup

Refractions through the sediment, crust, mantle, and reflections off the Moho described in section 3.2 above were used to invert for the velocity structure of the crust and upper mantle. The shots were projected onto a two-dimensional line with end points at 34.101°N, 83.760°W and 30.743°N, 81.706°W. The source receiver offsets were taken from the real geometry and assumed to fall along this 2-D line; thus, the true source-receiver offsets were preserved. This projection introduces some error particularly where there are large changes in basin structure over the scale of a couple of kilometers because (1) the assumption of 2-D

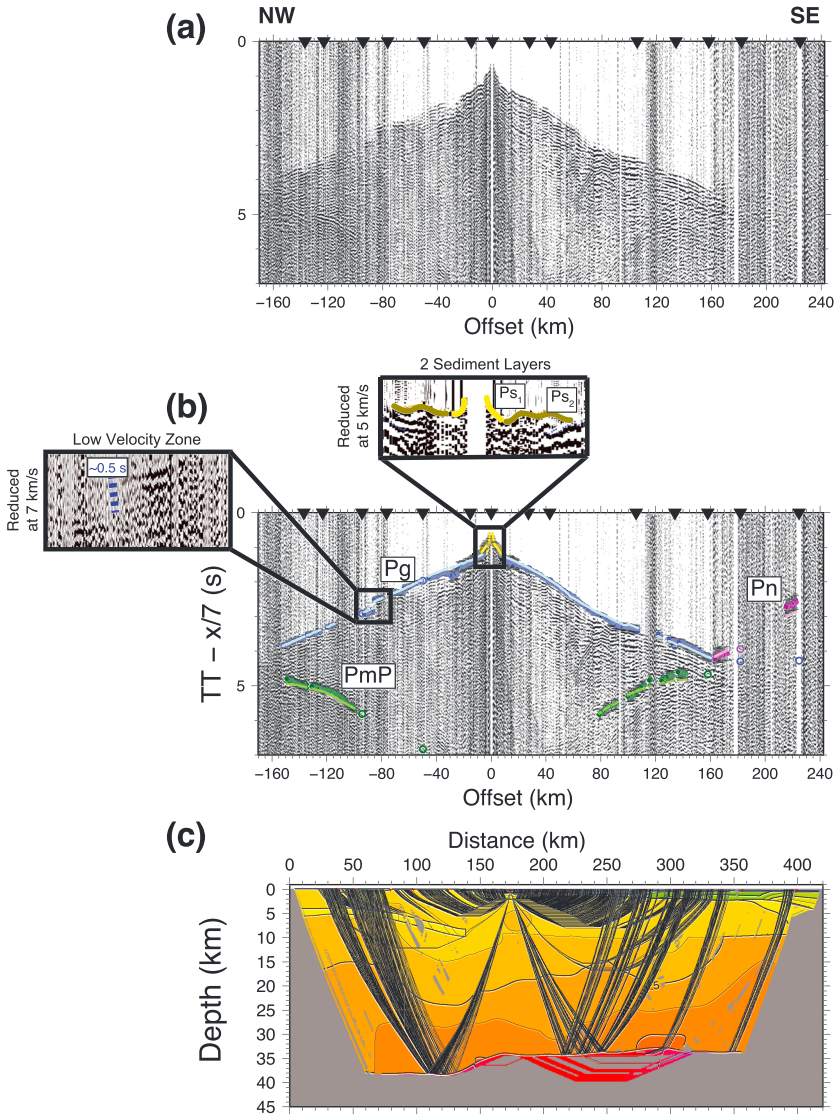

Figure 4. (a) Uninterpreted and (b) interpreted seismic data with *P* wave traveltime picks (dark color with error bars) and model calculated picks (pale color) from Shot 8 reduced at 7 km/s. Triangles above the *x* axes show the locations of other shots, and circles show reciprocity checks from picks on other shots. Top inset highlights the multilayered basin structure. Left side inset at −80 km highlights the delay in arrivals associated with the low-velocity zone. (c) Raypaths of the picked arrivals through the velocity model.

geometry is most likely to be incorrect at smaller source receiver offsets and (2) the regional basin structure is likely also three-dimensional and varies over spatial scales that are difficult to resolve precisely with our source and receiver spacing. The error introduced by projecting the slightly 3-D source-receiver geometry into a 2-D line, which can be expressed as the maximum variation in the location of a given receiver along the 2-D line for different shots, is usually less than 2 km but, in some cases, approaches 6 km. For this reason, larger uncertainties were often assigned to *Pg* and *Pn* picks near complex basins. The excellent correspondence of reciprocity checks of picks from different shots, which are calculated based on our 2-D geometry, shows that SUGAR Line 2 can be well modeled in two dimensions given some caution with the shallow basin structure.

3.4. Starting Model

Initial models for Line 2 were developed using RAYINVR, which uses a coarse velocity model parameterization with user-defined nodes (Zelt & Smith, 1992). We used this code for iterative forward modeling and

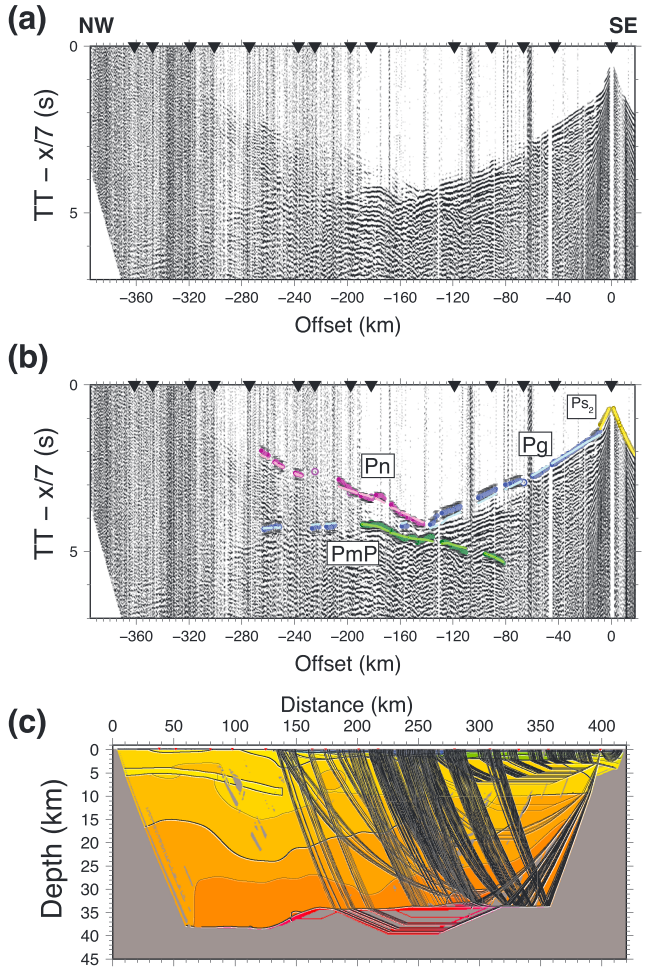

Figure 5. (a) Uninterpreted and (b) interpreted seismic data with *P* wave traveltime picks (dark color with error bars) and model calculated picks (pale color) from Shot 17 reduced at 7 km/s. Triangles above the *x* axes show the locations of other shots, and circles show reciprocity checks from picks on other shots. (c) Raypaths of the picked arrivals through the velocity model.

inversion to verify that phases were interpreted correctly, model the structure of basin sediments, and develop a 1-D starting model of the crust and upper mantle to combine with a forward modeled basin structure for finer-scale tomographic inversion modeling.

The basin structure was largely modeled in RAYINVR to incorporate both direct and indirect constraints on sediment velocities and thicknesses. The most direct constraints on basin structure from Line 2 are refractions through the sediment at small source-receiver offsets, but with an average shot spacing of 30 km, there were many gaps in coverage. To augment direct observations, we also use topography on *Pg* to further constrain basin structure. For example, higher basin thicknesses can be inferred where there is a consistent delay in *Pg* arrival times on multiple shots at a given distance along the 2-D line. Additionally, a sonic log from Well GGS-3080 between shots 10 and 12 constrained coastal plain and sedimentary basin velocities down to ~1.25-km depth (Chowns & Williams, 1983; J. Knapp, personal communication, Apr. 24, 2017). This forward modeled basin structure was then refined in the tomographic code VMTomo (e.g., van Avendonk et al., 1998; Roland et al., 2012; see following section).

The starting model for tomographic inversion included the basin structure, the approximate depth of the LVZ observed as a shadow zone in shot gathers, and average crustal and upper mantle velocities and depth to the base of the crust from forward modeling and inversion in RAYINVR described above. A 1-D crust and mantle velocity structure was assigned beneath the basin structure with a Moho depth set to 35 km. This starting modeling included an LVZ with a velocity and thickness that replicated the ~0.5-s traveltime delay observed in shots from the northern portion of the seismic line at ~80-km offset. Overall, we solved for smooth variations in crustal velocity with the tomographic inversion described in the next section, which did not allow the very steep vertical velocity gradients needed to explain this 0.5-s shadow zone to emerge unless a separate layer was included. We placed the low-velocity layer in the starting model deep enough for the crustal refractions arriving before the traveltime delay to travel above the LVZ at ~5 km and dipping slightly to the southeast, which approximately corresponds with an ~5- to 15-km-deep subhorizontal layer identified in other seismic studies near Line 2. In reflection seismic data, this layer appears as a highly reflective, laminated sequence (Cook & Vasudevan, 2006) and is modeled as an LVZ based on receiver functions from the SESAME passive source array (Parker et al., 2015). Because our data only provide information on where this low-velocity feature exists and the observed traveltime delay, there are tradeoffs between the velocity and thickness of this low-velocity layer. Ultimately, we selected a model with a relatively thick low-velocity layer with relatively high velocities (e.g., which would be consistent with sheared and/or metamorphosed sediments), which seemed more geologically feasible than a thin layer with very low velocities given available constraints on rock velocities (Johnston & Christensen, 1992). The lateral extent of the layer was estimated based on the distribution of records for which a shadow zone was observed.

Table 2
V_P Model Statistics

Ray type	Number of rays	RMS	χ^2
P_{sed}	441	0.0969	1.312
Pg	11,007	0.0753	0.987
PmP	3,271	0.0950	0.551
Pn	818	0.1380	0.923
Model Total	15,537	0.0848	0.901

Note. Model 12.124BIGLVZ.vm. RMS = root-mean-square.

3.5. Tomographic Inversion

Determination of the final velocity model entailed iterative ray tracing and inversion, with the goal of finding a smooth model that fits the traveltime data within its uncertainties. Updates to the model

Table 3
V_S Model Statistics

Ray type	Number of rays	RMS	χ^2
Sg	3,210	0.0865	1.6073

Note. Model S4.38.vm. RMS = root-mean-square.

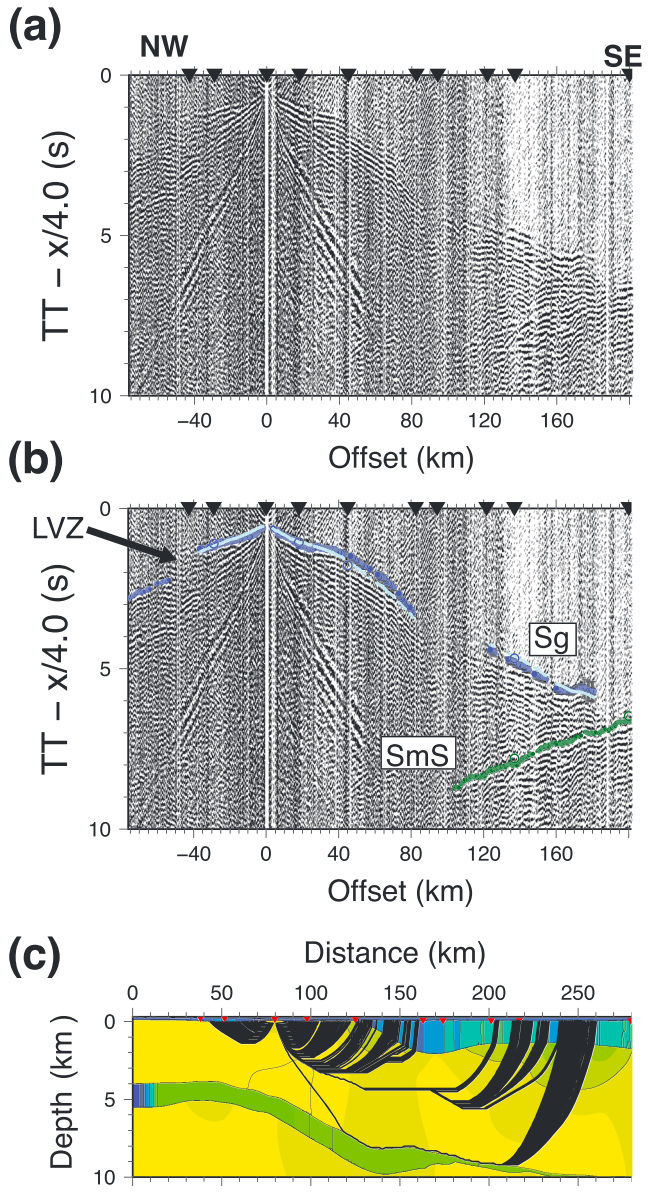

Figure 6. (a) Uninterpreted and (b) interpreted seismic data with *S* wave traveltime picks (dark color with error bars) and model calculated picks (pale color) from Shot 4 reduced at 4 km/s. Triangles above the *x* axes show the locations of other shots, and circles show reciprocity checks from picks on other shots. Arrow points to the low-velocity zone and possible reflections or refractions that travel to the base of or below the low-velocity zone. (c) Raypaths of the picked arrivals through the velocity model.

were based on a cost function that includes both data misfit and smoothing constraints. Using the RAYINVR-based starting model described in the previous section, we used the code VMTomo to invert for the velocity structure shown in Figure 2b.

The version of VMtomo that we used was first developed by H. van Avendonk and updated by A. Harding. Details about the method and code are described in multiple references (van Avendonk et al., 1998, 2004; Roland et al., 2012) and briefly summarized here. Models are parameterized using a slowness grid in which there are layer boundaries associated with laterally varying slowness jumps between layers. Rays are traced via the graph method through a 4,201 (x) by 654 (z) model grid (e.g., 0.1-km node spacing) to identify the shortest path from a source to the receivers given the ray type, which was either a refraction through a specified layer or a reflection off a specified boundary (Moser, 1991). In addition to grid spacing, ray tracing depends on the forward star, which defines the dimensions of the iterative grid search that seeks to identify the shortest traveltime path connecting grid nodes (Moser, 1991). The forward star varied during the inversion process but was, at minimum, six nodes across and nine nodes down.

The inversion algorithm uses damped least squares to reduce the difference between predicted and observed traveltimes in the layers of the model that are being inverted. As described in Roland et al. (2012), there is subjectivity in how the inversion parameters are selected, which include constraints on model flatness and smoothness in the horizontal and vertical directions and the relative amount of regularization for slowness jumps and layer boundary depths. The advantages of this flexible process are that inversion parameters can be modified between iterations, and iterations can be rerun with new parameters when nongeological structures and/or structures that increase the model misfit are introduced. To minimize nongeological structures that sometimes emerged from inversion like ray streaks or LVZs not required by the data, we either applied additional smoothing following inversion and/or modified the regularization parameters. At the start of the inversion, we used higher values for damping (e.g., 100), flatness (e.g., 20), and smoothness (e.g., 20) and lowered the values as the model fit to the data improved. We balanced the flatness and smoothness constraints and found that an aspect ratio of 5 or 10, allowing more regularization in the horizontal than vertical direction, resulted in the model converging in fewer iterations to a reasonable solution.

We used a layer-stripping approach to invert for the velocity structure. The sediment structure modeled in RAYINVR was held fixed, and we started inversions in the crust above the LVZ. We increased the uncertainty on *Pg* arrivals to values up to 0.25 s in portions of the model where basin thicknesses changed abruptly. Because of the shot spacing and slightly three-dimensional experiment geometry, these increases in uncertainty helped prevent the inversion from building basin-related traveltime delays into the velocity structure of the upper crust. Once the χ^2 for refractions through the upper crust was approximately 1, we inverted for lower crust velocity structure. After improving the fit for the lower crust, we added reflections off the Moho and refractions through the upper mantle and inverted jointly for the velocities in the lower crust, mantle, and Moho depth. After all layers of the model fit the data reasonably well, we refined the sediment structure and upper crust structure using rays through deeper parts of the model to constrain the inversion.

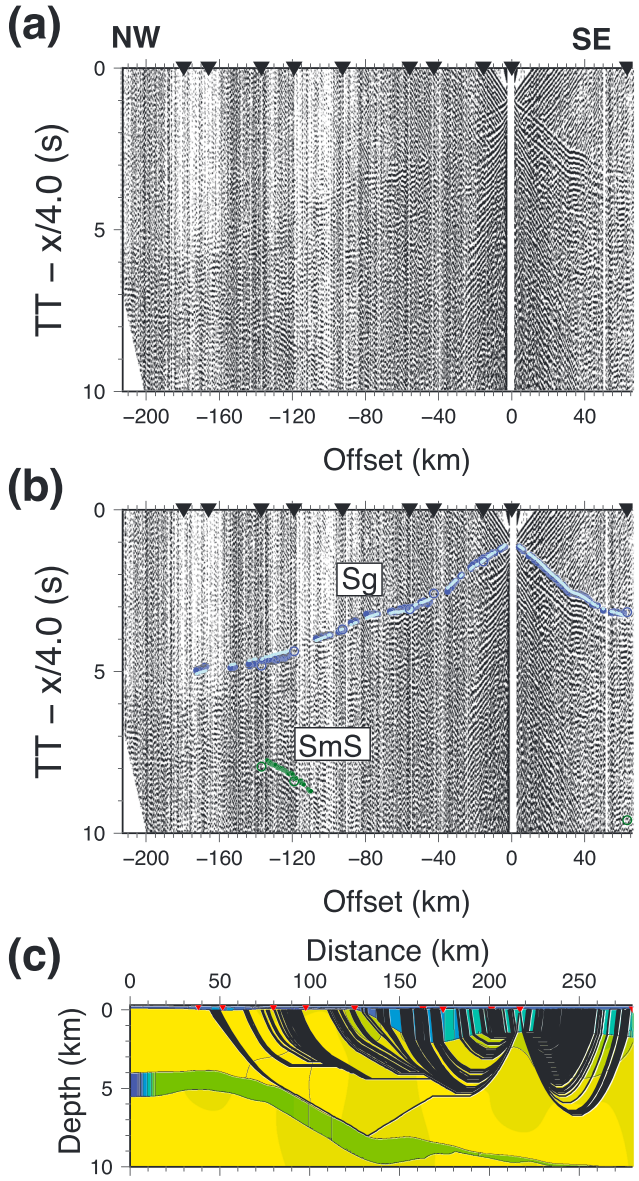

Figure 7. (a) Uninterpreted and (b) interpreted seismic data with *S* wave traveltime picks (dark color with error bars) and model calculated picks (pale color) from Shot 10 reduced at 4 km/s. Triangles above the *x* axes show the locations of other shots, and circles show reciprocity checks from picks on other shots. (c) Raypaths of the picked arrivals through the velocity model.

4. Results and Interpretation

4.1. V_P Model

Figure 2b shows the final *P* wave velocity model along SUGAR Line 2, which provides constraints on the sedimentary, crustal, and upper mantle structure beneath several major tectonic features in the SE United States. This model fits the data well with a relatively smooth velocity structure and a Moho boundary that is consistent with the Moho depth from analysis of passive-source seismic data (Schmandt et al., 2015). The final model has a chi-square value of 0.90 and an RMS (root-mean-square) misfit of 85 ms. Table 2 lists statistics of the fit between observed and predicted traveltimes for this model. Figures 3–5 show examples of arrival picks, the predicted traveltimes for the final model, and the rays traced through the model. North of the Higgins-Zietz magnetic boundary (0–125 km, Figure 2), we observe relatively high V_P crust above an LVZ at ~5-km depth. There is no significant sedimentary layer, and we observe the deepest Moho depths along the line at ~39 km. South of the Higgins-Zietz boundary, our seismic observations do not require a low-velocity layer. The crust is thinner, and the Moho is observed at depths of ~35 km. The sediment layer thickens to a maximum of 4 km. The data can be fit with a simple velocity structure without a large contrast in crustal velocities across the BMA. The following sections describe different portions of the model in more detail.

4.1.1. Sedimentary Structure

The final model includes two shallow layers with relatively low velocities that are interpreted as synrift and postrift sediment. Two layers were needed to satisfy the abrupt changes in velocity indicated by the apparent velocities of sedimentary refractions (e.g., Figure 4). The upper layer has velocities of 2.0–3.0 km/s and varies in thickness from 0 to 1.09 km. Comparison with nearby COCORP seismic reflection profiles indicate that this layer likely corresponds to a combination of coastal plain sediments and other underlying postrift sediments (McBride et al., 1987). The lower layer has higher and more variable velocities of 3.6–5.7 km/s and variable thickness of 0–4.1 km and is interpreted to primarily represent synrift sediments.

A couple of distinct areas of thicker sediments are observed along the line at 150 and 250 km (Figure 2), which we interpret as Mesozoic rift basins. The basin at 150 km (Figure 2c, profile ii) is characterized by a thin upper layer with lower (2–3 km/s) velocities overlying a thicker layer of higher velocities of ~5 km/s (Figure 4), whereas the basin at 250 km (Figure 2c, profile iii) includes ~1 km of sediments with similarly low (~2.5 km/s) velocities underlain by a thin <0.5-km layer of higher-velocity sediments. The velocity model for the basin at 250 km was further constrained by well log data (Chowns & Williams, 1983; J. Knapp, personal communication, 2017) very close to our line at model distance 250 km, which indicate velocities less than <3 km/s to depths of 1 km. The contrast in velocity between the sediments in these two basins suggests that their physical properties are different, likely because of contrasting sediment compaction levels and/or composition. These two basins are separated by an area of thin postrift sediments and minimal to no synrift sediments. To the south, starting at ~280 km, the sedimentary layer has a more constant thickness and velocity of ~4 km/s until it abruptly deepens and increases in velocity at a distance of ~400 km (Figure 2b).

The lateral extent of these sedimentary basins and their thicknesses are broadly consistent with those from previous studies. Constraints on sediment thicknesses from COCORP reflection seismic lines in eastern Georgia near Line 2 show two subbasins separated by a region with thin to absent synrift sediment

(McBride et al., 1987). The Riddleville Basin to the north is bounded by a southeast dipping fault and is up to 3 km deep (Petersen et al., 1984), which is consistent with our observations of this basin located ~150 km. A second basin is observed near the BMA that is at deepest ~1.5 TWTT, similar to the basin located at 250 km on SUGAR Line 2. Although the COCORP lines are offset from the SUGAR lines, maps of the extent of basin sediments constrained by drill data support two similarly located Triassic basins and identify diabase intrusions in the southeastern basin (Chowns & Williams, 1983).

4.1.2. Crustal Structure

The crustal velocity structure required to fit the data is surprisingly simple considering that this crust experienced multiple terrane accretion events during the Appalachian orogeny, CAMP magmatism, and extension during the breakup of Pangea. For the most part, crustal velocities range between 5.9 and 7.0 km/s and crustal thicknesses from the base of the sediments to the Moho range between 30.5 and 38.4 km. The average velocity for the full crust including the sediment is 6.2 ± 0.3 km/s, and the average velocity of crust excluding sediment is 6.5 ± 0.1 km/s. The crust was modeled as three layers to allow the inclusion of a low-velocity layer indicated by a shadow zone in the range 80- to 100-km offset on eight shots (e.g., Figure 4). The most notable lateral variation in velocity is observed in the upper crust (<10 km or above the LVZ), where the velocities on the northern part of the line are relatively high (~6.3 km/s) compared to crust at similar depths to the south (~6.1 km/s). The boundary between these two crustal domains occurs near the Higgins-Zietz boundary (Figure 2). The high-velocity crust in the north is a robust feature that is apparent from the slopes of refractions from the upper crust on this part of the line (Figures 3 and 4 at negative offsets). To the south, there is no apparent lateral change in the upper crustal velocity structure associated with the BMA.

Below the upper crust, we infer an LVZ in the northern portion of the line based on the observation of a shadow zone on multiple shots at similar offsets. It lies at a depth of 4–6 km, as constrained by the maximum offsets of arrivals above the shadow zone. Because no rays turn within the LVZ, there are significant tradeoffs between thickness and interval velocity structure. Our constraints on the LVZ structure are that (1) it introduces a traveltime delay at 80-km offset at positive offsets on shots 3–4 and at negative offsets on shots 5–10, (2) it underlies *Pg* arrivals that turn above the LVZ, and (3) the combination of its velocity and thickness results in a delay of ~0.5 s. From these constraints, we modeled a subhorizontal layer that deepens toward the south with a velocity ~5.5 km/s. The structure we model is broadly consistent with a structure at similar depths inferred from modeling of receiver functions (Parker et al., 2015) and from nearby COCORP reflection seismic data (Cook & Vasudevan, 2006). This represents a relatively thick, high-velocity end-member of the family of models that could satisfy the observed traveltime delay, which we considered most geologically likely. However, we note that a thinner, lower-velocity layer could also satisfy our observations.

The lower crust along Line 2 has a simple velocity structure with velocities generally ranging from 6.2 to 6.95 km/s. These velocities do not permit large volumes of mafic magmatic intrusions (e.g., Christensen & Mooney, 1995). Middle to lower crustal (>10 km or below the LVZ) velocities gently increase toward the southeastern end of the line, including maximum velocities of 7.15 km/s at 300-km distance, which implies a southward increase in any mafic magmatic addition. The Moho in the northwestern part of the line is deepest at ~39-km depth and shallows abruptly to ~34 km at 150-km distance, and then continues to shallow slightly to 300-km distance. Tradeoffs in the thickness versus interval velocity of the LVZ in the upper crust add uncertainty in the Moho depth beneath the LVZ, and the depth could be ~1 km shallower for a slower and thinner LVZ. The Moho in our model is consistently a few kilometers shallower than the Moho determined from a regional analysis of EarthScope data (Schmandt et al., 2015) but compares favorably with other wide-angle studies in the region. In the Carolina Terrane (at distances of ~80–120 km on Line 2), for example, average crustal thicknesses of ~38 km and average crustal velocities of 6.4 km/s are similar to crustal thicknesses of 37–39 km and average velocities of 6.5–6.6 km/s previously determined within the high-grade Kiokee belt of the Carolina Terrane (Hawman, 1996; Hawman et al., 2012).

Multiple crustal thickness estimates show the Moho shallowing and the crust thinning to the southeast (Parker et al., 2013, 2016; Schmandt et al., 2015). *SsPmp* constraints from SESAME data estimate crustal thickness beneath the coastal plain at 29.8 ± 2.0 km with an average crustal velocity of 6.5 ± 0.1 km/s (Parker et al., 2016). In comparison, estimates from the portion of the SUGAR seismic line beneath the coastal plain where Moho depth is resolved (130–350 km) suggest an average crustal thickness of 32.4 km but the same average basement velocity to 0.1 km/s precision. Variations in crustal thickness may reflect

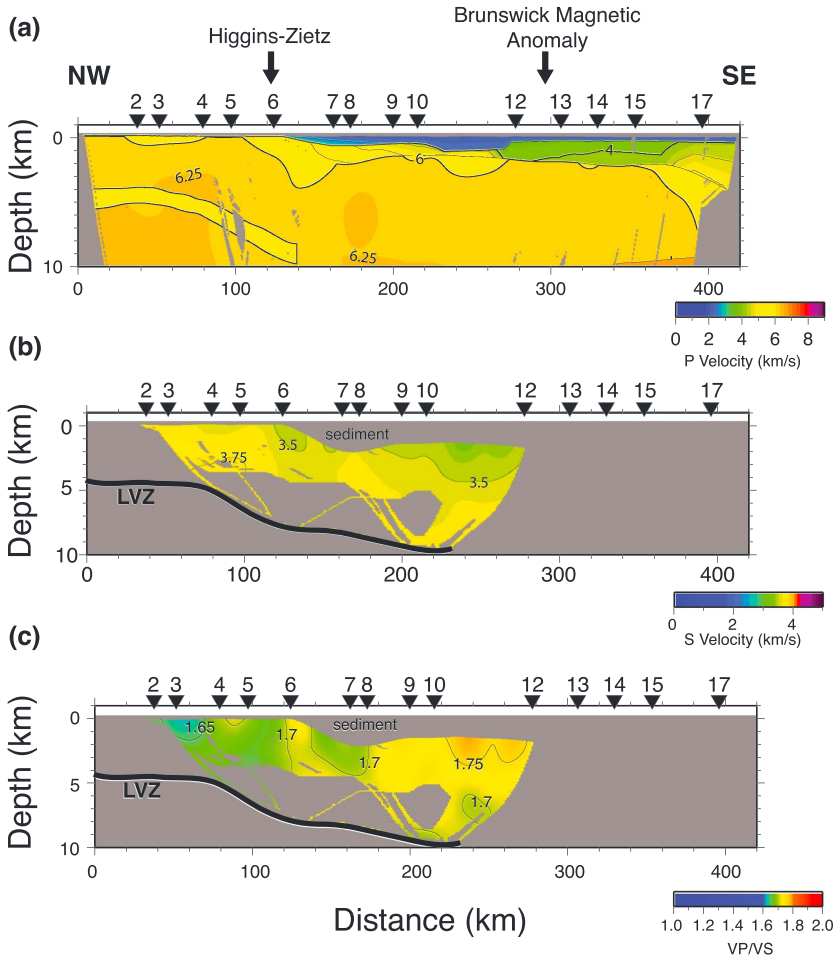

Figure 8. Inversion results for (a) *P* wave velocity, (b) *S* wave velocity, and (c) V_P/V_S of the upper crust, masked to show only parts of the model constrained by ray coverage. Notable magnetic anomalies are shown above the model.

differences in the locations and/or resolutions of the two data sets. Our higher-resolution constraints on Moho topography, however, show more concentrated shallowing at 150 km and then gradual crustal thinning toward the SE compared to prior crustal thickness estimates (Schmandt et al., 2015). The onset of this shallowing Moho coincides with the increase in sediment thickness and the Higgins-Zietz boundary.

Upper mantle velocities are constrained at line distances ~100–350 km by *Pn* arrivals. Velocities at line distances between ~150 and 300 km range from ~7.8 to 8.0 km/s, and velocities between ~100–150 and ~300–350 km range from ~8.0 to 8.3 km/s.

4.2. Upper Crustal V_S and V_P/V_S

Figure 8b shows the final V_S model for the upper crust. Figures 6 and 7 show examples of arrival picks, the picks predicted by the final velocity model, and the rays traced through the model. This model has a chi-square value of 1.6 and an RMS misfit of 87 ms. Table 3 lists model statistics for the V_S model. North of the Higgins-Zietz boundary, V_S reaches 3.75 km/s at 3-km depth compared to typical velocities of 3.5 km/s at 3-km depth south of the Higgins-Zietz boundary. The higher apparent velocities of near-offset *Sg* arrivals on Shot 4 compared to Shot 10 in Figures 6 and 7 show this change in upper crustal V_S. This decrease in upper crustal shear velocity south of the Higgins-Zietz boundary mirrors the decrease in upper crustal V_P (Figure 8a).

Figure 8c shows V_P/V_S in the upper crust based where velocities are constrained by ray coverage in both the V_P and V_S models. Values of V_P/V_S to the north of the Higgins-Zietz boundary above the LVZ are lower at

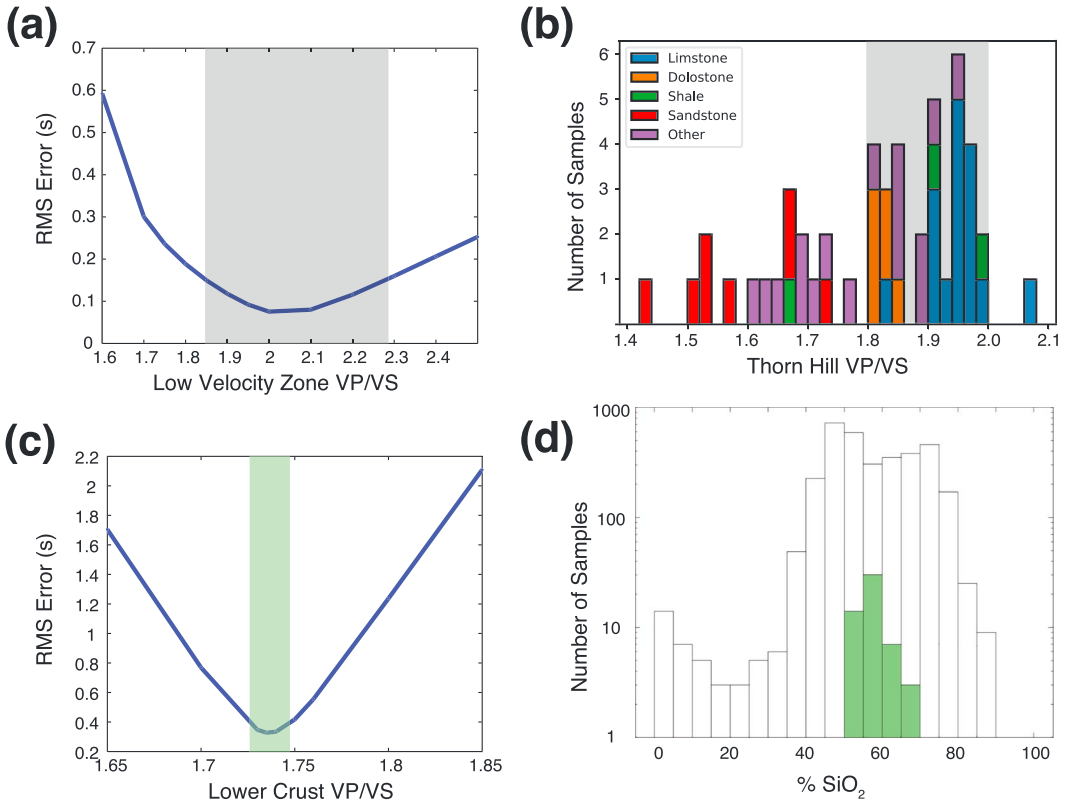

Figure 9. RMS error versus assumed V_P/V_S ratio for (a) the low-velocity zone, assuming a lower crust V_P/V_S of 1.739, and (c) the lower crust, assuming a low-velocity zone V_P/V_S of 2.0, where the gray highlighted portion represents the parameters that present an acceptable fit to the data. (b) V_P/V_S measurements from Paleozoic sedimentary rocks inferred to form the Appalachian detachment (Johnston & Christensen, 1992). (d) White bars show the histogram of SiO_2 content for a range of compositions (Hacker et al., 2015; Huang et al., 2013), and green bars show which of those samples have calculated V_P between 6.25 and 7.0 km/s and V_P/V_S between 1.73 and 1.74 at 1 GPa and 500 °C (Hacker et al., 2015), consistent with seismic constraints from SUwannee suture and GeorgiA Rift basin Line 2. RMS = root-mean-square.

1.65–1.7 than values to the south, which are 1.7–1.75. These values reflect the fact that, while both upper crustal V_P and V_S were higher to the north, the values of V_S increased more relative to V_P. Values of V_P/V_S in this upper crustal model compare favorably with prior estimates of upper crustal V_P/V_S using mine blasts that were largely in the range of 1.68–1.74 (Hawman et al., 2012).

4.3. Constraints on V_P/V_S in the LVZ and Lower Crust

In order to constrain V_S and V_P/V_S of the LVZ and lower crust where the *S* arrivals do not provide sufficient constraints to warrant a full tomographic inversion, we calculated predicted traveltimes and misfit with observed traveltimes for different constant V_P/V_S values in the layer of interest. We constructed V_S models using the V_S model for upper crust (section 4.2) and calculating V_S below from the V_P model (section 4.1) assuming a constant V_P/V_S for the layer of interest. To estimate V_P/V_S of the LVZ, we held other parts of the model fixed and varied V_P/V_S in the LVZ from 1.6 to 2.5. The V_S for the upper crust was taken from the final V_S model (Figure 8c), and V_S for the lower crust was calculated assuming a V_P/V_S ratio of 1.739 (determined as described below to be an appropriate fit). We calculated the misfit of the *Sg* arrivals below the LVZ on Shots 4 and 5 like those shown in Figure 6 at offsets < −40 km. Figure 9a shows that V_P/V_S values between 1.85 and 2.25 provide an RMS error less than 0.15 s, and the best fit is observed at a V_P/V_S of 2.0. From our data, we would not expect to resolve heterogeneities in the LVZ, so this analysis is designed to estimate average layer properties. Because this forward modeling test simplifies the fact that the LVZ is likely heterogeneous, and there is uncertainty in the pick arrivals, we consider V_P/V_S values that produce an RMS misfit below 0.15 to fit the data reasonably well. This range of plausible values is consistent with

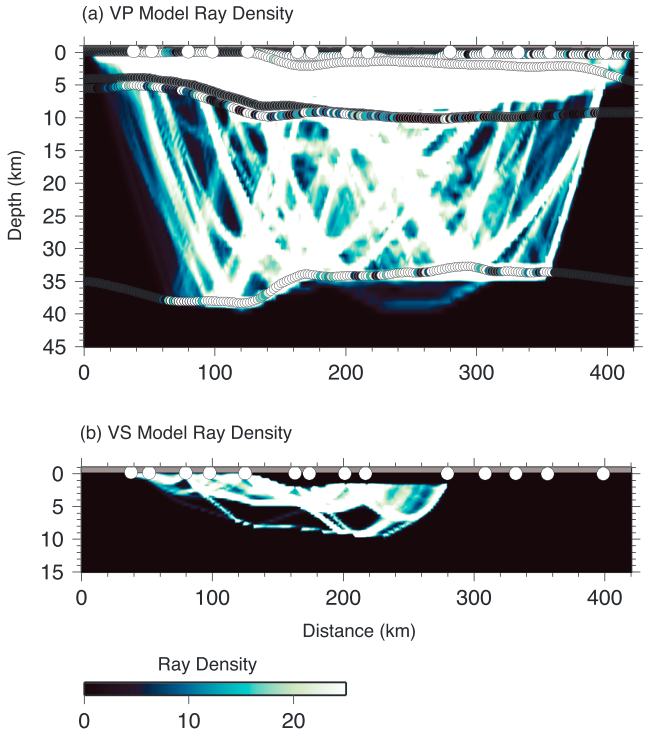

Figure 10. Derivative weight sum values for (a) the V_P model and (b) the V_S model, which measures ray density. White circles indicate shot locations. Colored circles at reflection boundaries indicate ray density at the reflection point on the same color scale as the derivative weight sum grid.

measurements of V_P/V_S from the Paleozoic sediments at 200 MPa inferred to form the Appalachian detachment that largely fall between 1.8 and 2.0 shown in Figure 9b (Johnston & Christensen, 1992).

Using the upper crustal V_S model and an assumed V_P/V_S of the LVZ of 2.0, we performed a similar analysis to determine the best fitting constant V_P/V_S for the lower crust based on *SmS* picks on Shots 4, 5, 6, 10, and 12. The results in Figure 9c show that the lower crust is best fit by a V_P/V_S ratio in the range of 1.73–1.74, where we observe an RMS misfit <0.4 s. These relatively low lower crustal V_P/V_S values are consistent with the low whole crust V_P/V_S values of 1.69–1.72 measured beneath the Carolina Terrane using receiver functions from SESAME broadband seismic data (Parker et al., 2013). At higher and lower V_P/V_S values, the RMS misfit rises sharply, though the relatively high RMS misfit even at V_P/V_S of 1.735 likely reflects heterogeneity in lower crustal V_P/V_S that is not captured by a constant lower crust V_P/V_S value. The white bars in Figure 9d show the distribution of SiO_2 values for a range of granulite and amphibolite-facies terrain and xenolith compositions (Hacker et al., 2015; Huang et al., 2013) for which seismic velocities were calculated with Perple_X at 1 GPa and 500° (Hacker et al., 2015). The green bars show the subset of those compositions with V_P between 6.25 and 7.0 km/s and V_P/V_S between 1.73 and 1.74, consistent with seismic velocities observed in the middle to lower crust on SUGAR Line 2. Because these compositions all have between 50% and 70% SiO_2, we can infer that the lower crust beneath Line 2 has an average intermediate to felsic, not mafic, composition.

4.4. Model Uncertainty and Resolution

The uncertainty and resolution of the tomographic models depends strongly on ray coverage resulting from traveltime picks. Figure 10 shows the derivative weight sum (DWS) for the V_P and V_S models, which reflects the density of ray coverage at each given point in the model. DWS values in the V_P model are highest in the upper crust and have nonzero values down to the upper mantle. In the V_S model, DWS values are high in the upper crust down to ~5–10 km at line distances of 40–280 km, with very little ray coverage outside this region.

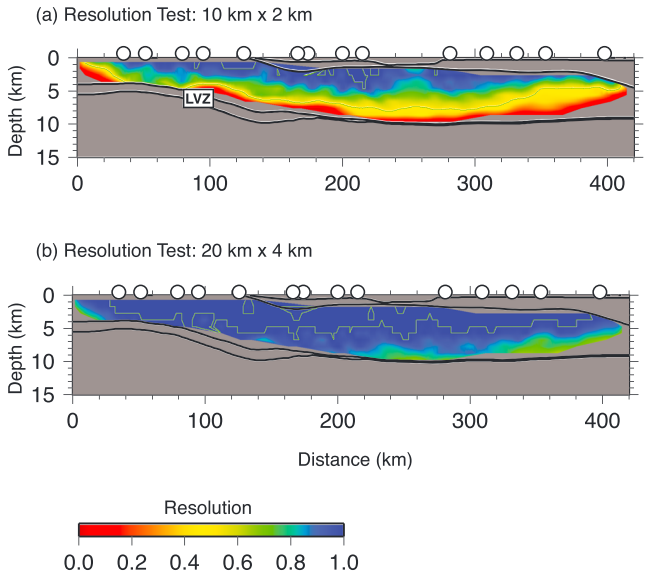

Figure 11. V_P upper crust resolution tests at two scales in the form of horizontal × vertical length: (a) 10 × 2 km and (b) 20 × 4 km. Values greater than 0.5 can be interpreted as acceptable resolution. White circles indicate shot locations. LVZ = low-velocity zone.

In addition to raypath density, the diagonal of the resolution matrix quantifies the degree to which a given point in the inverted velocity model is smearing a broader area in the true model (van Avendonk et al., 2004). This depends on ray coverage and on inversion parameters including damping, smoothing, vertical versus horizontal regularization, and velocity versus layer boundary regularization. We use the resolution matrix to assess how well different sized elliptical features in the model are resolved with the methods in van Avendonk et al. (2011) for the V_P model of the upper crust (Figure 11), lower crust and mantle (Figure 12), and V_S model of the upper crust (Figure 13). Portions of the model not constrained by ray coverage are shaded in gray. In this analysis, resolution values >0.5 indicate that an anomaly of the given size is resolvable by the inversion given the data (van Avendonk et al., 2011). Figure 11 shows that 10 × 2-km upper crustal V_P anomalies are well resolved, which is more than adequate to constrain the upper crustal velocity contrasts on either side of the BMA and Higgins-Zietz boundary.

We run a similar set of resolution tests for the joint inversion of the lower crustal velocity, Moho depth, and upper mantle velocity, using larger ellipses because velocity resolution decreases in the deeper portions of

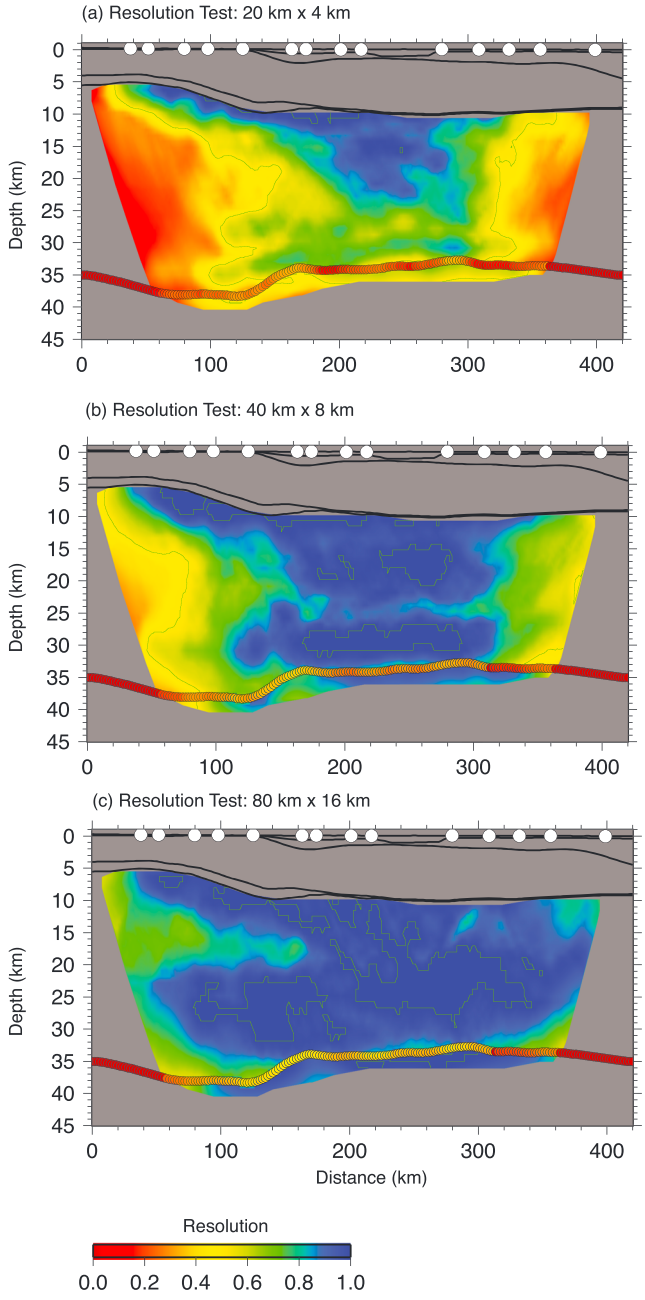

Figure 12. V_P lower crust and upper mantle resolution tests at three larger length scales: (a) 20 × 4 km, (b) 40 × 8 km, and (c) 80 × 16 km. Values greater than 0.5 can be interpreted as acceptable resolution. White circles indicate shot locations. The resolution of the Moho reflector is shown by circles colored with the same color scale as the resolution grid.

the model. Figure 12 shows that velocity anomalies in the lower crust and upper mantle are well resolved at spatial scales of 40 × 8 km in the center of the model, and of 80 × 16 km toward the edges of the model; lower resolution is expected near the edges of the model due to less ray coverage and the absence of reversed ray coverage. The Moho interface is best resolved at the center of the velocity model, where it is constrained by reversed ray coverage. Interpreting the resolution of the Moho interface in relation to lower crust and upper mantle velocities is not straightforward because a smaller number of rays refract through the lower crust, reducing velocity constraints in this part of the model. Thus, there are tradeoffs between increasing the velocity of the lower crust and increasing the Moho depth to fit *PmP* arrivals and the onset of *Pn*.

Figure 13 shows resolution tests for the upper crust V_S model using the same three length scales tested for the upper crust V_P model in Figure 11. These resolution tests show that our data resolve velocity anomalies at spatial scales of at least 10 × 2 km through most portions of the model with ray coverage. The model resolution is highest at the top of the crust and at distances between 60 and 280 km. Because our constraints on sediment structure are limited to traveltime delays until the onset of *Sg*, one source of uncertainty that is not reflected in these resolution tests is the sediment velocity structure. The onset of near-offset *Sg* constrains average V_S structure in the sediments near shots where we picked *Sg* (2–12; line distances 40–280 km), but the sediment structure is less constrained between shots and is poorly constrained south of Shot 12.

Because the LVZ is an important but prescribed model feature, it is important to discuss (1) the influence of this feature on surrounding velocities and (2) constraints on the feature itself. Outside the LVZ, the density of *Pg* ray coverage above and below the LVZ is a strong indicator of the sensitivity to the depth and geometry of the LVZ. In particular, velocities above the LVZ are well constrained by *Pg* arrivals and are unlikely to change significantly in response to changing the position of the LVZ in ways that are consistent with the data. These arrivals also place some constraints on the depth to the top of the LVZ. There are uncertainties in the thickness and V_P, V_S, and V_P/V_S of the LVZ due to tradeoffs between thickness and velocity, and in the extent of the LVZ due to ~20- to 30-km shot spacing. We thus integrate indirect observations from SUGAR data and other data sets to develop our preferred model (section 3.4). The relative delays in *P* and *S* wave arrivals constrain V_P/V_S within the LVZ in a way that is relatively independent of the exact placement of the LVZ. Agreement between the properties of the LVZ from our data and other studies (e.g., Cook & Vasudevan, 2006; Johnston & Christensen, 1992; Parker et al., 2015) supports the constraints that we do place on the seismic properties of the LVZ. Finally, the LVZ increases uncertainty in the underlying crustal velocities compared to other parts of the model (Figure 10), particularly in the northernmost part of the model where there is less reversed ray coverage. In summary, despite inherent challenges associated with LVZs, we are able to develop a geologically reasonable model for LVZ structure and geometry using constraints from SUGAR data and other complementary data sets.

5. Discussion

The velocity models presented above are the first detailed crustal velocity models that extend across the Inner Piedmont, Carolina Terrane, a couple of possible Paleozoic sutures from past orogenies, and the

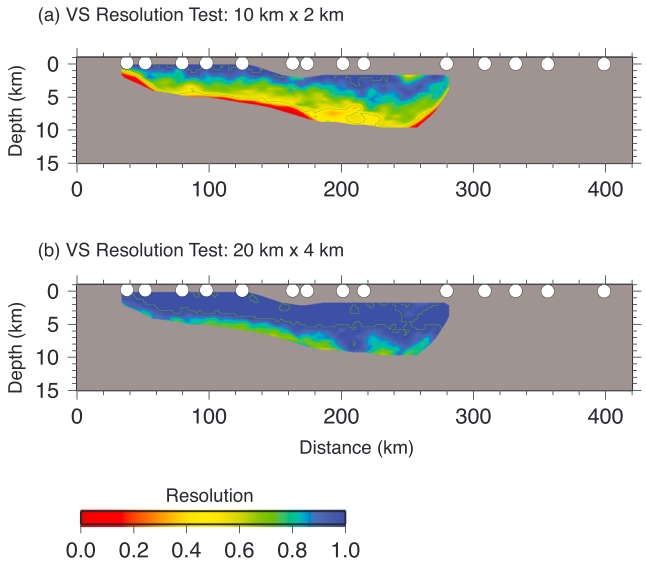

Figure 13. V_S upper crust resolution tests at two scales: (a) 5 × 1 km and (b) 10 × 2 km. Values greater than 0.5 can be interpreted as acceptable resolution. White circles indicate shot locations.

Mesozoic South Georgia Rift Basin. The crustal velocity structure on Line 2 provides new constraints on (1) the terrane composition and style of terrane accretion that formed the southern Appalachians, (2) the relationships between preexisting weak suture zones and extension that formed the South Georgia Basin, and (3) how these orogenic and rift-related structures influence the locations of earthquakes in this region today.

5.1. Terrane Accretion in the Southern Appalachians

5.1.1. Velocity Changes Between Terranes

Velocities from SUGAR Line 2 provide new constraints on the physical properties of the accreted terranes, the boundaries between terranes, and the detachment beneath them. Here we combine these observations with existing constraints from structural and compositional analysis of rocks at the Earth's surface to the north of coastal plain and from drill sites within the coastal plain, reflection seismic data, receiver functions, and a patchwork of wide-angle refraction seismic constraints from mine blasts. Our new model, combined with these complementary data sets, shows that there is a contrast in upper crustal composition that aligns approximately with the Higgins-Zietz boundary and that, to the north of this boundary, relatively high-velocity terranes that are ~3–5 km thick overlie a reflective, low-velocity and/or anisotropic layer interpreted to be a detachment.

The northern end of Line 2 crosses the Inner Piedmont and Carolina terranes (e.g., Hatcher et al., 2007; Merschat & Hatcher, 2007; Secor et al., 1983). In relation to terrane boundaries based on surface geology, the upper crust beneath Shots 2, 3, and 4 is associated with the Inner Piedmont and the upper crust beneath Shots 5 and 6 is associated with the Carolina terrane (Figures 1 and 14a). Analysis of surface geology suggests that the Inner Piedmont is characterized by high-grade metamorphic rocks and mafic rocks (Goldsmith et al., 1988; Griffin, 1971). Rock assemblages include sillimanite-grade rocks in the core of the Inner Piedmont and less metamorphosed kyanite-grade rocks dominated by amphibolite and granitoid gneiss at the northwestern and southeastern flanks. The Carolina Terrane, located southeast of the Inner Piedmont, is an amalgam of multiple subterranes that likely docked onto Laurentia together (Hibbard et al., 2002) and includes metavolcanic rocks associated with a primitive island arc sequence (Whitney et al., 1978). The metamorphic grade of rocks varies between subterranes, but amphibolite facies rocks are observed in the Charlotte belt and greenschist facies rocks in the Carolina Slate Belt (e.g., Secor et al., 1986; Shervais et al., 2003).

In the V_P and V_S models, upper crustal velocities of terranes north of the Higgins-Zietz boundary, especially the Inner Piedmont terrane, are higher than those to the southeast, which is consistent with the relatively high metamorphic grade of the Inner Piedmont. V_P of upper crust decreases from 6.0–6.3 km/s beneath Shots 2–4 in the Inner Piedmont to 5.9–6.1 km/s at comparable depths south of the Higgins-Zietz boundary (Figure 2). V_S also decreases to the south of the Higgins-Zietz boundary, and V_P/V_S increases. The contrast in V_P/V_S from north to south might be related to differences in porosity and/or quartz content, both of which change V_P/V_S.

Overall, V_P/V_S values from this study are within 0.05 of the values calculated in prior work by dividing the arrival times of *P* and *S* arrivals on individual traces from mine blasts (Hawman et al., 2012). The sparse data analyzed by this prior work, however, could not identify a change in V_P/V_S across the Higgins-Zietz boundary. The linear geometry and denser source-receiver spacing from the SUGAR experiment allow us to base V_P/V_S measurements on 2-D velocity models and do not assume that the *P* and *S* arrival on a given trace traveled through the same path through the crust.

Remarkably, we do not observe any significant changes in V_P associated with the BMA. We do not have constraints on V_S south of the BMA so cannot assess any possible changes in V_S or V_P/V_S across the BMA.

Our observation of a significant change in upper crustal velocity at the Higgins-Zietz boundary is consistent with recent analysis that points to it as the location of the suture that separates pre-Alleghanian Laurentia

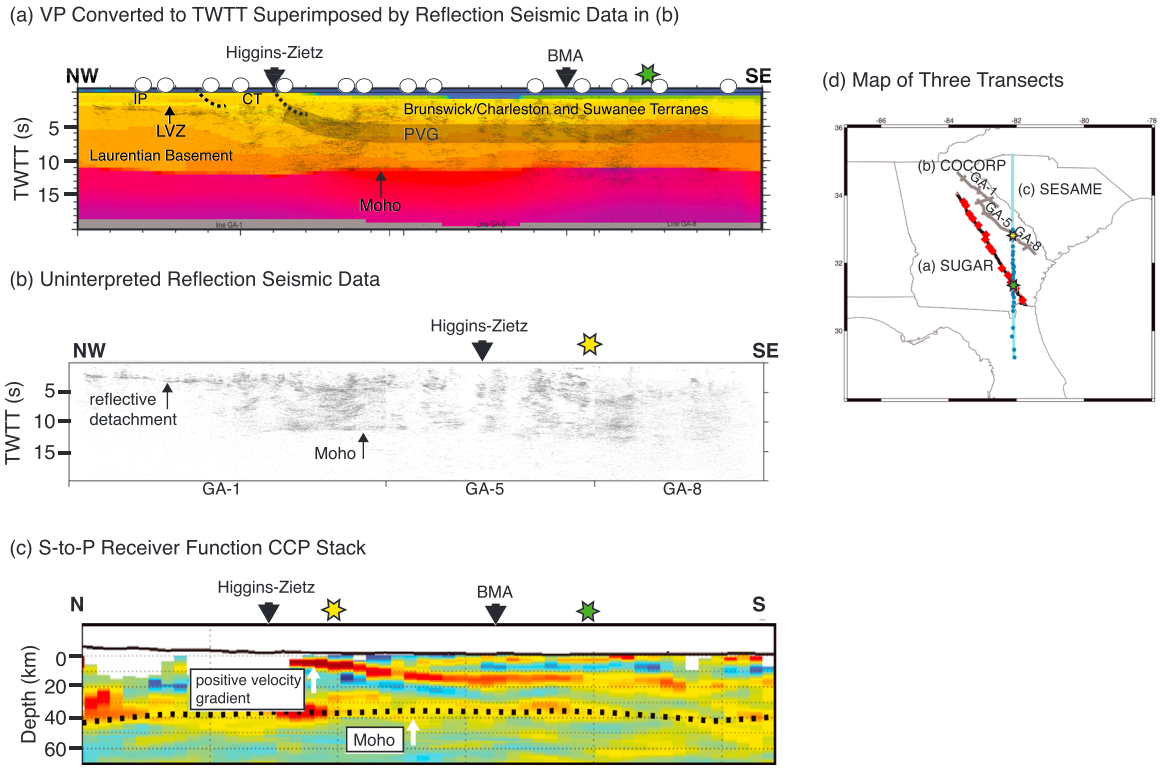

Figure 14. Constraints on the structure of the Appalachian detachment from three geophysical data sets from this region, which are close together but not exactly colocated. (a) Appalachian detachment is a low-velocity zone in the SUGAR V_P model. The z axis is converted to TWTT for direct comparison with nearby COCORP reflection seismic data, plotted above the velocity model. The positive velocity gradient from plot (c) is shown approximately by the thick gray line. Velocities are plotted with the same color bar as in Figure 5, and white circles above the velocity model show shot locations. (b) Uninterpreted COCORP reflection seismic data lines GA-1, GA-5, and GA-8 (Cook & Vasudevan, 2006), showing the Appalachian detachment as a slightly SE dipping reflective, laminated layer at ~2–4 s TWTT. (c) S to P receiver function CCP stack for line B from the SESAME experiment (Hopper et al., 2017), showing the detachment as a south dipping positive velocity gradient at ~5- to 15-km depth. (d) Map of the relative locations of the three data sets. Green and yellow stars on all panels show crossings between the profiles. SUGAR = SUwannee suture and GeorgiA Rift basin; TWTT = two-way traveltime; COCORConsortium for Continental Reflection Profiling; SESAME = Southeastern Suture of the Appalachian Margin Experiment.

from the terranes that docked onto the Laurentian margin during the Alleghanian assembly of Pangea. Receiver function imaging from the SESAME project has revealed a dipping structure that appears to shallow at the Higgins-Zietz boundary (Figure 14c; Hopper et al., 2017). Additional evidence for this boundary comes from constraints on the northwestern extent of undeformed sediments in the Gondwanan-affinity Paleozoic Suwannee Basin from legacy seismic and well data (Boote & Knapp, 2016). Because the Suwannee basin predates the Alleghanian orogeny and extends, undeformed, northwest of the BMA, the suture zone between Laurentia and Gondwana should also be located northwest of the BMA. These findings suggest that the contrast in V_P/V_S across the Higgins-Zietz boundary characterizes a contrast in upper crust composition between the Gondwanan terranes in the southeast and the high-grade metamorphosed rocks and mafic arc rocks to the northwest.

5.1.2. Seismic Properties of the Appalachian Detachment

The LVZ in the V_P model provides an additional constraint on the properties of the detachment over which the Inner Piedmont and Carolina Terranes accreted onto Laurentia. Figure 14 shows images of the SUGAR Line 2 V_P model converted from depth to TWTT (Cook & Vasudevan, 2006), the uninterpreted COCORP reflection seismic data, and the S to P receiver function CCP (common conversion point) stack from Line B of the SESAME experiment (Hopper et al., 2017). Although the three data sets sample similar geologic structures, the map inset shows they are not colocated, which could account for the relatively small differences in the depth or time to a given structure. The northern portions of all three data sets show a layer in the shallow crust at ~5-km depth that dips slightly to the southeast. Between the three data sets, characteristics of this feature include that (1) the layer introduces a ~0.5-s traveltime delay in P wave refraction

seismic data (Figures 4a and 4b), limiting its thickness to <2 km, (2) it is a reflective layer in the multichannel seismic reflection data (e.g., Cook & Vasudevan, 2006), and (3) it generates a positive velocity gradient in the receiver function image (Hopper et al., 2017). The fact that the detachment layer generates a positive velocity gradient and an LVZ is consistent with the interpretation from Hopper et al. (2017) of the boundary being radially anisotropic. Alternatively, or additionally, the receiver functions may be more sensitive to the increase in velocities at the base of this layer compared with the decrease in velocities at the top of it. In addition to the seismic data shown in Figure 14, forward models to fit *P-SV* converted phases required an LVZ in the V_S structure starting at ~5-km depth beneath the Inner Piedmont and 12-km depth beneath the Carolina terrane (Parker et al., 2015). Heat flow data from the Appalachian Ultradeep Core Hole site are also consistent with a detachment depth of ~5 km (Costain & Decker, 1987).

The properties of the low-velocity, anisotropic layer of deformed metasediments inferred from seismic data are consistent with laboratory measurements of the metasediments that outcrop in the Valley and Ridge, thought to underlie the Appalachian accreted terranes (Johnston & Christensen, 1992). Some of these samples have low *P* wave velocities between 4.0 and 6.0 km/s. Additionally, in these rocks, anisotropy ranges from 0% to 60%, with most samples having anisotropy between 0% and 10%.

Approaching the Higgins-Zietz boundary at a distance of 100–120 km (Figures 2 and 14), the detachment layer appears to dip more steeply in all data sets. Farther south, receiver functions are interpreted to indicate that the detachment continues into the midcrust and extends near-horizontally beyond the BMA and into Florida (Hopper et al., 2017). However, the LVZ observed in the SUGAR data appears to terminate at the Higgins-Zietz boundary and not continue farther south. COCORP seismic reflection data include some subhorizontal reflections at a similar depth to the midcrustal feature in the receiver function images south of the Higgins-Zietz (Cook & Vasudevan, 2006) but do not include any reflections as bright and continuous as those marking the Appalachian detachment to the north of the Higgins-Zietz boundary. It is important to note that north of the Higgins-Zietz boundary, the detachment underlies the Inner Piedmont and Carolina terranes and was most active during the Neoacadian orogeny when the Cat Square terrane of the Inner Piedmont and the Carolina Terrane accreted onto Laurentia (Bream et al., 2004; Carrigan et al., 2003; Huebner et al., 2017), though it likely reactivated and was subject to significant displacement during the later Alleghenian orogeny (Hibbard, 2000). If the Higgins-Zietz boundary does indeed mark the Alleghanian suture, any detachment to the south of this boundary would underlie the Charleston and Suwanee terranes and would have only been active during the Alleghenian orogeny.

There are three possible end-member explanations for why we do not observe evidence in SUGAR refraction seismic data for the midcrustal detachment southeast of the Higgins-Zietz boundary: (1) SUGAR data do not sample an LVZ associated with this detachment because the layer is too deep in the crust or the crustal refractions are sampling the LVZ fast axis (horizontally); (2) the properties of the midcrustal detachment change where it deepens and underlies the Charleston and Suwannee terranes south of the Higgins-Zietz boundary such that we do not observe it (Figures 15b–15d); or (3) the detachment that underlies the Inner Piedmont and Carolina terranes does not continue south of the Higgins-Zietz boundary (Figures 15e–15 g). The first scenario is unlikely because we observe *Pg* to large offsets and would expect to see a shadow zone if an LVZ persisted farther south and to greater depths.

Option (2) suggests that even though the Appalachian suture is a continuous feature, its seismic properties change along its length such that it can be divided into two components. The portion north of the Higgins-Zietz boundary reflects terrane accretion onto the Laurentian margin primarily during the Neoacadian orogeny, where metasedimentary passive margin sediments generate the reflective, high V_P/V_S and low-velocity layer beneath the Inner Piedmont and Carolina terranes. The southern section, which is not observed in our refraction seismic data, may represent a more metamorphosed and seismically faster sedimentary layer, and/or a midcrustal shear zone formed as the Charleston and Suwannee terranes were thrust onto Laurentia during the Alleghenian orogeny (Hopper et al., 2017). In this case, velocity variations at the shorter scale lengths important for generating continuous, high-amplitude reflections in active source data may not be present. This scenario is also consistent with the laterally continuous velocities in the middle and lower crust, which do not show any sharp changes that might be expected across a steeply dipping boundary and thus could imply a continuation of Laurentian crust to the south.

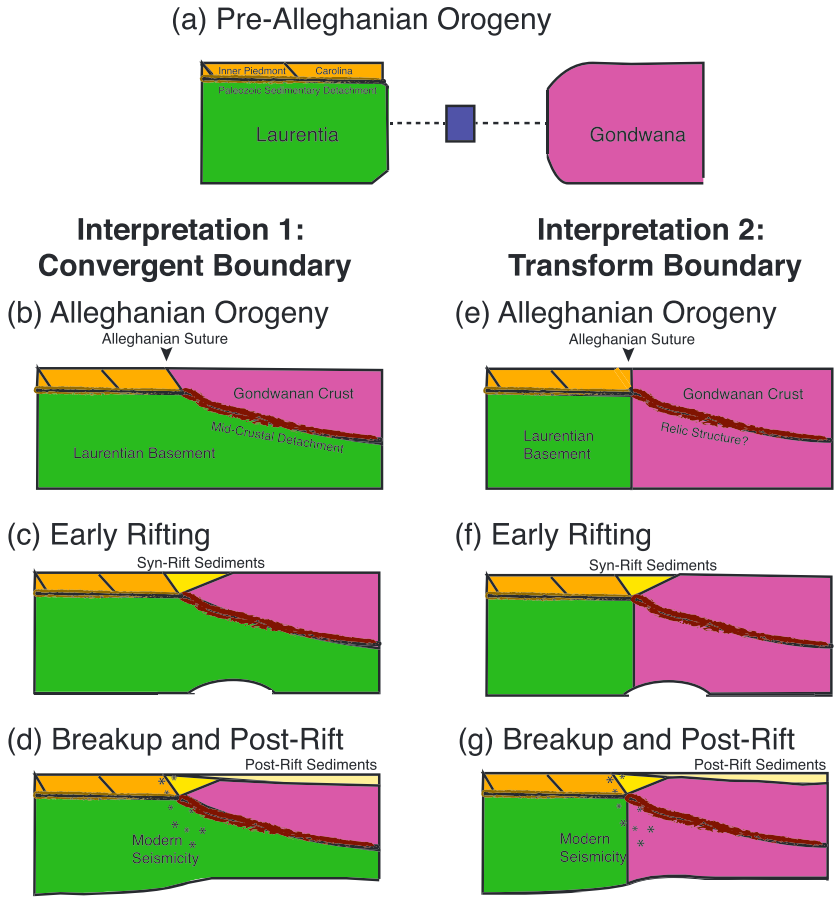

Figure 15. Interpretation of the evolution of the southeastern U.S. crust if the Alleghanian suture is a (b–d) shallowly dipping convergent boundary (Option 2 in text) or (e–g) near-vertical strike-slip boundary (Option 3 in text). (a) Before the Alleghanian orogeny, through (b, e) orogenesis and (c, f) rifting to (d, g) the present.

Option (3) interprets the southward termination of the LVZ in our model and the bright, continuous reflection in COCORP reflection data to mean that the detachment does not continue farther south and is instead truncated by a steeply dipping Alleghenian suture, as inferred by Cook & Vasudevan (2006; Figure 15). A steeply dipping structure was imaged in COCORP seismic data near the Higgins-Zietz boundary in western Georgia where it merges with the BMA and interpreted as the Alleghenian suture (McBride, 1991), but no steeply dipping structures are imaged in any of the regional passive or active source seismic imaging studies at the Higgins-Zietz boundary in eastern Georgia where it is separate from the BMA (Cook & Vasudevan, 2006; McBride, 1991). Instead, steeply dipping reflections are only observed farther south beneath the BMA. Steeply dipping structures are challenging to image with seismic reflection techniques, so it is possible that such a feature is present beneath the Higgins-Zietz boundary but not imaged. Small earthquakes described in section 5.3 do appear to occur in a relatively steeply dipping band consistent with a near-vertical suture. This option, however, requires another explanation for the prominent midcrustal structure observed in receiver functions (Hopper et al., 2017; e.g., that it is a relict feature from a previous tectonic event).

The results from SUGAR Line 2, alone, cannot distinguish between these two end-member options. In either case, it is interesting to note that we do not observe a relatively fast midcrustal layer in our V_P model that would be predicted by a radially anisotropic midcrustal layer interpreted from the receiver function images.

The geological record of the Alleghenian orogeny in the southeastern United States provides clues that are interpreted to support either significant orthogonal collision (e.g., Hatcher, 2002) that could be consistent with a gently dipping detachment or transpression (e.g., Pollock et al., 2012; Secor et al., 1986) that would be consistent with a steeply dipping structure. Many reconstructions include multiple phases of deformation

(e.g., strike-slip deformation followed orthogonal collision; Hatcher, 2010). Here we briefly summarize a couple of key lines of geological evidence for each end-member. Alleghenian-aged metamorphism and deformation is observed over a large lateral extent in the eastern United States, consistent with significant orthogonal collision (e.g., Hnat & van der Pluijm, 2014; Tull et al., 2007). On the other hand, a transpressional regime is interpreted based on structural analysis and isotopic dating of Alleghanian shear zones (Gates et al., 1986, 1988) and the lack of evidence for subduction-related magmatism (Mueller et al., 2014). Some reconstructions involve strike-slip deformation throughout the orogen during the earlier phases, followed by continued strike-slip deformation in the northern Appalachians and more thrust deformation in the southern Appalachians as collision occurred from north to south and Gondwana swung into Laurentia (Hatcher, 2002, 2010).

If hundreds of kilometers of collision occurred along a gently dipping detachment at ~20- to 30-km depth, as interpreted by Hopper et al. (2017), what happened to the Gondwanan and Laurentian lower crust and upper mantle? As described by Hopper et al. (2017), low-grade andalusite-bearing shales from boreholes southeast of the suture limit the burial depths of rocks presently at the surface to ~10 km (Milton, 1972). This limits the thickness of Gondwanan crust above the suture at the time of convergence to <30 km. Geodynamic models suggest that if the lower crust is weak enough or thick enough, it can decouple from the upper crust and delaminate (Chemenda et al., 2000). Some of the Laurentian crust beneath the imaged midcrustal detachment would also need to have been removed through delamination or other processes to reach its present-day thickness. The Pb isotope geochemistry of CAMP dikes in the southeastern United States has been interpreted to include lower crust contamination of the mantle magma source (Callegaro et al., 2013; Marzoli et al., 2018; Whalen et al., 2015), which could reflect such removal of Laurentian lower crust. Despite the geodynamic questions above that are raised by this interpretation, it is difficult to ignore the fact that images of some modern orogenies like the Himalayas include shallow, gently dipping detachments similar to the one interpreted by Hopper et al. (2017) in the southern Appalachians (Schulte-Pelkum et al., 2005).

In summary, the geometry of the Alleghenian suture and the style of orogenesis remain uncertain and controversial. While the SUGAR Line 2 results provide strong evidence for the manifestation of the Alleghenian suture in the upper crust, they cannot directly constrain its geometry at depth. Based on geological evidence for both strike-slip and collisional deformation during the Alleghenian orogeny and given the prominence and continuity of a major midcrustal feature imaged by receiver functions over a large region, we favor a model involving earlier strike-slip deformation followed by collision to form a gently dipping midcrustal detachment (Option 2). However, the data presented here are also consistent with Option 3; thus, we cannot rule it out.

5.2. Relationship Between Suture Zones and Rift Localization

The patterns in crustal thickness, crustal velocities, and basin structure can be used to examine the influence of preexisting structures on rifting and magmatism. At ~120-km distance on Line 2, we observe the Riddleville rift basin, an increase in V_P/V_S indicating a change in upper crustal properties across the Higgins-Zietz boundary, which we interpret as the Alleghanian suture, and a decrease in crustal thickness (Figure 2). These observations suggest that extension localized along either the Alleghanian boundary marked by the Higgins-Zietz boundary or in the accreted crust to the south.

Although magmatism can be an important factor in facilitating rifting by weakening the lithosphere (Buck, 2006), there is limited evidence for significant magmatic addition along Line 2, particularly beneath the South Georgia Basin. Mafic synrift magmatic intrusions would increase the seismic velocity of the crust, and estimates for the velocity of intruded mafic rocks based on offshore seismic observations range from 7.2 to 7.5 km/s (Lizarralde et al., 1994; Trehu et al., 1989). Although a mix of intruded mafic rocks and the original lower crust might result in lower crust velocities less than 7.2 km/s, there is no localized increase in lower crustal velocity beneath the primary rift basins of the South Georgia Rift or near the suture zone, and lower crust velocities are almost entirely <7.0 km/s. These observations suggest that synrift magmatism was limited during extension to form the South Georgia Basin. This interpretation is consistent with the relative timing of extension that formed the South Georgia Basin and the dates of magmatic intrusions in the southeastern United States. The timing of rifting inferred from dates on sediments in the South Georgia Basin is ~230–205 Ma (Withjack et al., 2012), while high-resolution dates on magmatic intrusions from

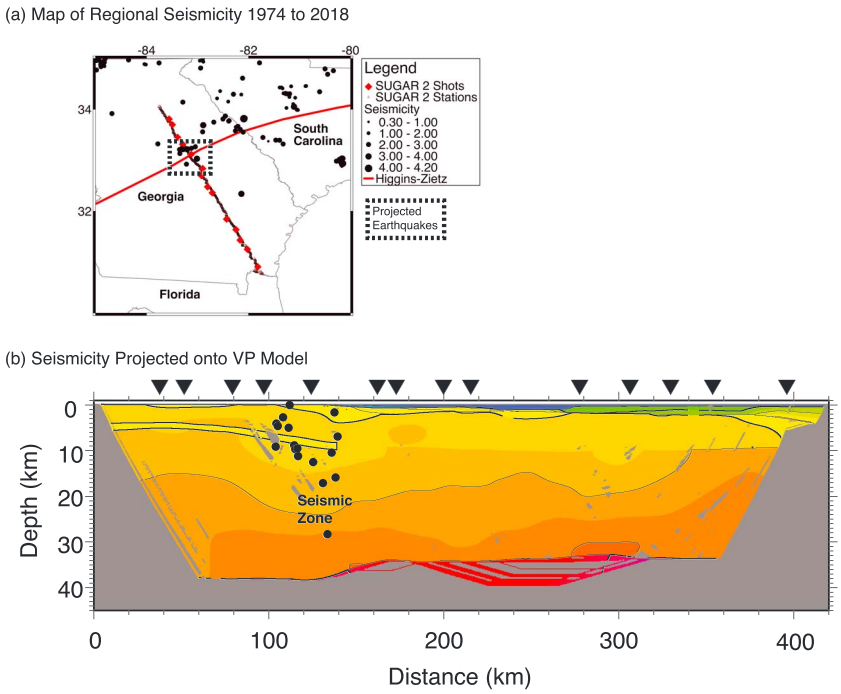

Figure 16. (a) Map of seismicity between 1974 and January 2018 from the CERI New Madrid seismic catalog (http://www.memphis.edu/ceri/seismic/catalog.php) with event symbols scaled by magnitude. Earthquakes inside the dotted line box were projected onto the SUGAR Line 2. (b) The cross-sectional view of seismicity plotted on the Line 2 V_P model. SUGAR = SUwannee suture and GeorgiA Rift basin.

this time period are from CAMP at ~201 Ma (Blackburn et al., 2013; Callegaro et al., 2013). It also implies that there was not volumetrically significant magmatic addition to the crust after rifting during CAMP. We do observe a gentle increase in middle to lower crustal velocities toward the Georgia coast at the southeastern end of the seismic line. The simplest explanation for this increase given its location is the emplacement of some mafic magmatic intrusions during continental breakup.

There are two end-member mechanisms through which rifting may have localized in relation to the Alleghanian suture. In the first mechanism, extension may have exploited an orogenic fault zone at the Higgins-Zietz boundary. The main uncertainty with this mechanism is that the geometry of the Alleghenian structure(s) at depth is (are) uncertain, as described in the previous section. If steeply dipping structures that penetrate much of the crust are present, these may be well oriented to be reactivated during extension. Alternatively, extensional faulting could have exploited shallow contrasts in crustal properties and weaknesses associated with a shallow, gently dipping structure. The second mechanism through which extension might have been localized by preexisting structures is through the concentration of strain within the Suwannee and Charleston terranes. In this scenario, the rheological properties of these terranes may have made them easier to extend than the Laurentian crust, both during the formation of the South Georgia Basin and during the breakup of Pangea. We cannot distinguish between these two possibilities, but our observation of crustal thinning focused south of the Higgins-Zietz boundary implies a control by the configuration created by orogenesis on later rift development.

The crust remains relatively thin to the southeastern extent of the seismic line. We interpret this pattern as the result of two stages of thinning. During the first stage, extension to form South Georgia Basin was localized beneath Riddleville basin and the other rift basin at 250 km in the model. In the second stage, later extension that lead to rupture of Pangea further thinned crust nearest to the rifted margin on the southeastern end of our seismic line.

5.3. Controls of the Appalachian Detachment on Central Georgia Seismicity

The southeastern United States is seismically active today with a principal stress orientation that reflects a balance between stresses from glacial isostatic adjustment and ridge push from the Mid-Atlantic Ridge. In

central Georgia, the maximum horizontal stresses are oriented in the azimuth range 51–65° (Zoback, 1992). Based on available data, the maximum horizontal stress orientation favors reactivating thrust faults with trends oriented approximately NW/SE and strike slip faults with trends approximately 30° from the maximum horizontal stress direction listed above.

Seismic activity in the SE United States is poorly understood, and prior studies have suggested multiple possible controls, including higher uplift rates near Atlanta, GA (Bollinger, 1973), the increase in dip or southeastern termination of the Appalachian detachment (Seeber & Armbruster, 1981), and structural weakening induced by elevating the water table (Costain et al., 1987). Events from the CERI (Center for Earthquake Research and Information) earthquake catalog (http://www.memphis.edu/ceri/seismic/catalog.php) between 1974 and January 2018 are projected onto the V_P model for Line 2 in Figure 16 to show the relationship between local seismicity and preexisting tectonic structures. Local seismicity concentrates where the Appalachian detachment dips most steeply in multiple data sets (Figure 14), including our model, and near a southeast dipping fault that bounds the Riddleville basin (Petersen et al., 1984). The colocation of seismicity with these two important features in our model indicates they may exert a control on modern seismicity. However, depending on the geometry of rifting and orogenic structures at depth, which are not well constrained by this study, the mechanism may be more complicated than simply reactivating either of these structures (Figure 15). Additional controlling factors may include the formation of new faults that selectively use portions of nonideally orienting preexisting fault planes (e.g., the most steeply dipping portion of the Appalachian detachment; e.g., Pratt et al., 2015; Viola et al., 2004) or that local perturbations to the stress field by preexisting faults promote faulting near these features (e.g., Morley, 2010).

6. Conclusions

In this paper, we present 2-D V_P and V_S crustal velocity models from SUGAR Line 2 that extend from the Inner Piedmont to near the Georgia coast. These velocity models provide new constraints on the crustal structures that formed in the Appalachians over multiple orogenies and the role of those structures in localizing subsequent rifting and present-day seismicity. Figure 15 shows the sequence of events that we interpret to have shaped the crust along Line 2. First, we interpret changes in V_P, V_S, and V_P/V_S in the upper crust at the Higgins-Zietz boundary as further supporting evidence that this is the Alleghanian suture between pre-Alleghanian Laurentia (Figure 15a) and the Brunswick/Charleston and Suwanee terranes that collided into Laurentia during the Alleghanian orogeny (Figures 15b and 15e). The Inner Piedmont and Carolina terranes north of the Higgins-Zietz boundary lie above an interpreted metasedimentary detachment at ~5-km depth. The shallowing Moho and synrift basin located just south of the change in properties at the Higgins-Zietz boundary suggest that rifting that formed the South Georgia Basin ~230–205 Ma localized either at the suture or in the accreted terranes to the south (Figures 15c and 15f). Surprisingly, there is limited evidence in the crustal velocity structure for magmatic intrusions, despite the widespread evidence for CAMP magmatism in near-surface geological and geophysical data onshore (Chowns & Williams, 1983; McBride et al., 1989) and in crustal velocity models offshore (Lizarralde et al., 1994). After this early phase of rifting and CAMP magmatism, the successful breakup of Pangea appears to have further thinned the crust at the southern end of SUGAR Line 2 (Figures 15d and 15 g). Today, a steeply dipping zone of seismicity in central Georgia that extends from the near surface to the lower crust cuts across the Appalachian detachment at the Alleghanian suture, which coincides with where the detachment dips most steeply and the northern edge of the South Georgia Rift Basin. This suggests that present-day intraplate stresses and seismicity may localize on or near the Alleghanian suture and/or faults bounding the northern edge of the South Georgia Rift.

Acknowledgments
The SUGAR experiment would not have been possible without the help of local landowners, county and state officials, the University of Texas El Paso seismic source facility, IRIS PASSCAL instrument center, and the team of students who scouted, deployed, and recovered the geophones. We thank Jim Knapp, Susie Boote, and Ross Cao for helpful discussion and providing the sonic log data from GGS-3080; Lindsay Worthington for discussion and sharing codes; Bradley Hacker and Mark Behn for sharing their lower crust velocity constraints; Emily Hopper and Karen Fischer for discussions; and Fred Cook for an image of processed COCORP data. We used the PyVM toolbox from Nathan Miller, the VMTomo code from Alistair Harding for tomographic inversions, VMTomo code from Harm van Avendonk for resolution tests, and the Upicker package of MATLAB scripts maintained by W. Wilcock to pick arrivals. Seismic Unix was used for data processing (Cohen & Stockwell, 2002). This project was funded by an NSF GRFP fellowship DGE 16-44869 and a grant from the National Science Foundation's Division of Earth Sciences (NSF-EAR) EarthScope program through the collaborative awards EAR-1144534, EAR-1144829, and EAR-1144391. Robert Hawman and two anonymous reviewers provided thorough feedback that improved this manuscript. The refraction seismic data set analyzed in the current study is available on request through the IRIS Data Management Center, report number 14-023 (http://ds.iris.edu/ds/nodes/dmc/forms/assembled-data/). The velocity model grid files and arrival picks are available in the supporting information.

References

Barnes, A. E., & Reston, T. J. (1992). A study of two mid-crustal bright spots from southeast Georgia (USA). *Geophysical Journal International*, *108*(2), 683–691. https://doi.org/10.1111/j.1365-246X.1992.tb04647.x

Beaumont, C., & Ings, S. J. (2012). Effect of depleted continental lithosphere counterflow and inherited crustal weakness on rifting of the continental lithosphere: General results. *Journal of Geophysical Research*, *117*, B08407. https://doi.org/10.1029/2012JB009203

Blackburn, T. J., Olsen, P. E., Bowring, S. A., McLean, N. M., Kent, D. V., Puffer, J., et al. (2013). Zircon U-Pb geochronology links the end-Triassic extinction with the Central Atlantic Magmatic Province. *Science*, *340*(6135), 941–945. https://doi.org/10.1126/science.1234204

Bollinger, G. (1973). Seismicity and crustal uplift in the southeastern United States. *American Journal of Science*, *273-A*, 396–408.

Boote, S. K., & Knapp, J. H. (2016). Offshore extent of Gondwanan Paleozoic strata in the southeastern United States: The Suwannee suture zone revisited. *Gondwana Research*, *40*, 199–210. https://doi.org/10.1016/j.gr.2016.08.011

Bream, B. R., Hatcher, R. D., Miller, C. F., & Fullagar, P. D. (2004). Detrital zircon ages and Nd isotopic data from the southern Appalachian crystalline core, Georgia, South Carolina, North Carolina, and Tennessee: New provenance constraints for part of the Laurentian margin. In R. P. Tollo, L. Corriveau, J. McLelland, & M. J. Bartholomew (Eds.), *Proterozoic Tectonic Evolution of the Grenville Orogen in North America* (Vol. 197, pp. 459–475). Boulder, Colorado: Geological Society of America Memoir.

Buck, W. R. (2006). The role of magma in the development of the Afro-Arabian Rift System. *Geological Society, London, Special Publications*, *259*(1), 43–54. https://doi.org/10.1144/GSL.SP.2006.259.01.05

Callegaro, S., Marzoli, A., Bertrand, H., Chiaradia, M., Reisberg, L., Meyzen, C., et al. (2013). Upper and lower crust recycling in the source of CAMP basaltic dykes from southeastern North America. *Earth and Planetary Science Letters*, *376*, 186–199. https://doi.org/10.1016/j.epsl.2013.06.023

Carrigan, C. W., Miller, C. F., Fullagar, P. D., Bream, B. R., Hatcher, R. D., & Coath, C. D. (2003). Ion microprobe age and geochemistry of southern appalachian basement, with implications for Proterozoic and Paleozoic reconstructions. *Precambrian Research*, *120*(1-2), 1–36. https://doi.org/10.1016/S0301-9268(02)00113-4

Chapman, M. C., Beale, J. N., Hardy, A. C., & Wu, Q. (2016). Modern seismicity and the fault responsible for the 1886 Charleston, South Carolina, earthquake. *Bulletin of the Seismological Society of America*, *106*(2), 364–372. https://doi.org/10.1785/0120150221

Chemenda, A. I., Burg, J.-P., & Mattauer, M. (2000). Evolutionary model of the Himalaya-Tibet system: Geopoem based on new modelling, geological and geophysical data. *Earth and Planetary Science Letters*, 397–409.

Chenin, P., Manatschal, G., Lavier, L. L., & Erratt, D. (2015). Assessing the impact of orogenic inheritance on the architecture, timing and magmatic budget of the North Atlantic rift system: A mapping approach. *Journal of the Geological Society*, *172*(6), 711–720. https://doi.org/10.1144/jgs2014-139

Chowns, T. M., & Williams, C. T. (1983). Pre-Cretaceous rocks beneath the Georgia coastal plain—Regional implications. In G. S. Gohn (Ed.), *Studies Related to the Charleston, South Carolina, Earthquake of 1886—Tectonics and Seismicity*, *U.S. Geological Survey Professional Paper* (Vol. 1313, pp. L1–L42).

Christensen, N. I., & Mooney, W. D. (1995). Seismic velocity structure and composition of the continental crust: A global view. *Journal of Geophysical Research*, *100*(B6), 9761–9788. https://doi.org/10.1029/95JB00259

Cohen, J. K., & Stockwell, J. J. W. (2002). *CWP/SU: Seismic Un*x: An Open Source Software Package for Seismic Research and Processing*. Golden, CO: Center for Wave Phenomena, Colorado School of Mines.

Coltice, N., Phillips, B. R., Bertrand, H., Ricard, Y., & Rey, P. (2007). Global warming of the mantle at the origin of flood basalts over supercontinents. *Geology*, *35*(5), 391. https://doi.org/10.1130/G23240A.1

Cook, F. A., Albaugh, D. S., Brown, L. D., Kaufman, S., Oliver, J. E., & Hatcher, R. D. (1979). Thin-skinned tectonics in the crystalline southern Appalachians; COCORP seismic-reflection profiling of the Blue Ridge and Piedmont. *Geology*, *7*(12), 563–567. https://doi.org/10.1130/0091-7613(1979)7<563:TTITCS>2.0.CO;2

Cook, F. A., & Vasudevan, K. (2006). Reprocessing and enhanced interpretation of the initial COCORP southern Appalachians traverse. *Tectonophysics*, *420*(1–2), 161–174. https://doi.org/10.1016/j.tecto.2006.01.022

Costain, J. K., Bollinger, G., & Speer, J. A. (1987). Hydroseismicity—A hypothesis for the role of water in the generation of intraplate seismicity. *Geology*, *15*(7), 618–621. https://doi.org/10.1130/0091-7613(1987)15<618:HHFTRO>2.0.CO;2

Costain, J. K., & Decker, E. D. (1987). Heat flow at the proposed Appalachian ultradeep core hole (ADCOH) site: Tectonic implications. *Geophysical Research Letters*, *14*(3), 252–255. https://doi.org/10.1029/GL014i003p00252

Daniels, D. L. (2001). Georgia aeromagnetic and gravity maps and data: A Web site for distribution of data. Retrieved from https://pubs.usgs.gov/of/2001/of01-106/

Deckart, K., Bertrand, H., & Liégeois, J.-P. (2005). Geochemistry and Sr, Nd, Pb isotopic composition of the Central Atlantic Magmatic Province (CAMP) in Guyana and Guinea. *Lithos*, *82*(3–4), 289–314. https://doi.org/10.1016/j.lithos.2004.09.023

Dunbar, J. A., & Sawyer, D. S. (1989). How preexisting weaknesses control the style of continental breakup. *Journal of Geophysical Research*, *94*(B6), 7278–7292. https://doi.org/10.1029/JB094iB06p07278

Gates, A. E., Simpson, C., & Glover, L. III (1986). Appalachian Carboniferous dextral strike-slip faults: An example from Brookneal, Virginia. *Tectonics*, *5*(1), 119–133. https://doi.org/10.1029/TC005i001p00119

Gates, A. E., Speer, J. A., & Pratt, T. L. (1988). The Alleghanian southern Appalachian Piedmont: A transpressional model. *Tectonics*, *7*(6), 1307–1324. https://doi.org/10.1029/TC007i006p01307

Gernigon, L., Brönner, M., Roberts, D., Olesen, O., Nasuti, A., & Yamasaki, T. (2014). Crustal and basin evolution of the southwestern Barents Sea: From Caledonian orogeny to continental breakup. *Tectonics*, *33*, 347–373. https://doi.org/10.1002/2013TC003439

Ghosh, A., Holt, W. E., & Bahadori, A. (2019). Role of large-scale tectonic forces in intraplate earthquakes of central and eastern North America. *Geochemistry, Geophysics, Geosystems*, *20*, 2134–2156. https://doi.org/10.1029/2018GC008060

Goldsmith, R., Milton, D. J., & Horton, J. W. J. (1988). Geologic Map of the Charlotte 1° × 2° Quadrangle. North Carolina and South Carolina.

Griffin, V. S. J. (1971). The Inner Piedmont belt of the Southern Crystalline Appalachians. *Geological Society of America Bulletin*, *82*(7), 1885–1898. https://doi.org/10.1130/0016-7606(1971)82[1885:TIPBOT]2.0.CO;2

Hacker, B. R., Kelemen, P. B., & Behn, M. D. (2015). Continental lower crust. *Annual Review of Earth and Planetary Sciences*, *43*(1), 167–205. https://doi.org/10.1146/annurev-earth-050212-124117

Hames, W. E., Renne, P. R., & Ruppel, C. (2000). New evidence for geologically instantaneous emplacement of earliest Jurassic Central Atlantic magmatic province basalts on the North American margin. *Geology*, *28*(9), 859–862. https://doi.org/10.1130/0091-7613(2000)28<859:NEFGIE>2.0.CO;2

Hatcher, R. D. (2002). Alleghanian (Appalachian) orogeny, a product of zipper tectonics: Rotational transpressive continent-continent collision and closing of ancient oceans along irregular margins. In J. R. Martinez Catalan, R. D. Hatcher, R. Arenas, & F. Diaz Garcia (Eds.), *Varsican-Appalachian Dynamics: The Building of the Late Paleozoic Basement* (pp. 199–208). Boulder, Colorado: Geological Society of America.

Hatcher, R. D. (2010). The Appalachian orogen: A brief summary. In R. P. Tollo, M. J. Bartholomew, J. P. Hibbard, & P. M. Karabinos (Eds.), *From Rodinia to Pangea: The lithotectonic Record of the Appalachian Region*, *Geological Society of America Memoir* (Vol. 206, pp. 1–19). https://doi.org/10.1130/2010.1206(01)

Hatcher, R. D., Bream, B. R., & Merschat, A. J. (2007). Tectonic map of the southern and central Appalachians: A tale of three orogens and a complete Wilson cycle. In *4-D Framework of Continental Crust*, *Geological Society of America Memoir* (Vol. 200, pp. 595–632). https://doi.org/10.1130/2007.1200(29)

Hatcher, R. D., & Merschat, A. J. (2006). The Appalachian Inner Piedmont: An exhumed strike-parallel, tectonically forced orogenic channel. In R. D. Law, M. P. Searle, & L. Godin (Eds.), *Channel Flow, Ductile Extrusion and Exhumation in Continental Collision Zones*, *The Geological Society of London Special Publications* (Vol. 268, pp. 517–541). https://doi.org/10.1144/GSL.SP.2006.268.01.24

Hawman, R. B. (1996). Wide-angle, three-component seismic reflection profiling of the crust along the East Coast Gravity High, southern Appalachians, using quarry blasts. *Journal of Geophysical Research*, *101*(B6), 13,933–13,945. https://doi.org/10.1029/96JB00792

Hawman, R. B., Khalifa, M. O., & Baker, M. S. (2012). Isostatic compensation for a portion of the southern Appalachians: Evidence from a reconnaissance study using wide-angle, three-component seismic soundings. *Geological Society of America Bulletin*, *124*(3–4), 291–317. https://doi.org/10.1130/B30464.1

Hibbard, J. P. (2000). Docking Carolina: Mid-Paleozoic accretion in the southern Appalachians. *Geology*, *28*(2), 127–130. https://doi.org/10.1130/0091-7613(2000)28<127:DCMAIT>2.0.CO;2

Hibbard, J. P., Miller, B. V., Hames, W. E., Standard, I. D., Allen, J. S., Lavallee, S. B., & Boland, I. B. (2012). Kinematics, U-Pb geochronology, and $^{40}Ar/^{39}Ar$ thermochronology of the Gold Hill shear zone, North Carolina: The Cherokee orogeny in Carolinia, southern Appalachians. *Geological Society of America Bulletin*, *124*(5–6), 643–656. https://doi.org/10.1130/B30579.1

Hibbard, J. P., Stoddard, E. F., Secor, D. T., & Dennis, A. J. (2002). The Carolina Zone: Overview of Neoproterozoic to Early Paleozoic peri-Gondwanan terranes along the eastern flank of the southern Appalachians. *Earth-Science Reviews*, *57*(3-4), 299–339. https://doi.org/10.1016/S0012-8252(01)00079-4

Higgins, M. W., & Zietz, I. (1983). Geologic interpretation of geophysical maps of the pre-Cretaceous "basement" beneath the coastal plain of the southeastern United States. *Geological Society of America Memoirs*, *158*, 125–130. https://doi.org/10.1130/MEM158-p125

Hnat, J. S., & van der Pluijm, B. A. (2014). Fault gouge dating in the southern Appalachians, USA. *Geological Society of America Bulletin*, *126*(5-6), 639–651. https://doi.org/10.1130/B30905.1

Hooper, R. J., Hatcher, R. D., Troyer, P. K., Dawson, R. J., & Redmont, C. G. (1997). The character of the Avalon terrane and its boundary with the Piedmont terrane in central Georgia. In L. Glover, III, & A. E. Gates (Eds.), *Central and Southern Appalachian Sutures: Results of the EDGE Project and Related Studies*, *Special Paper* (Vol. 314, pp. 1–14). Boulder, Colorado: Geological Society of America. https://doi.org/10.1130/0-8137-2314-0.1

Hopper, E., Fischer, K. M., Wagner, L. S., & Hawman, R. B. (2017). Reconstructing the end of the Appalachian orogeny. *Geology*, *45*(1), 15–18. https://doi.org/10.1130/G38453.1

Horton, J., Drake, A., & Rankin, D. (1989). Tectonostratigraphic terranes and their Paleozoic boundaries in the central and southern Appalachians. In R. D. Dallmeyer (Ed.), *Terranes in the Circum-Atlantic Paleozoic Orogens*, *Special Paper* (Vol. 230, pp. 213–245). Boulder, Colorado: Geological Society of America. https://doi.org/10.1130/SPE230-p213

Huang, Y., Chubakov, V., Mantovani, F., Rudnick, R. L., & McDonough, W. F. (2013). A reference Earth model for the heat-producing elements and associated geoneutrino flux. *Geochemistry, Geophysics, Geosystems*, *14*, 2003–2029. https://doi.org/10.1002/ggge.20129

Huebner, M. T., Hatcher, R. D., & Merschat, A. J. (2017). Confirmation of the southwest continuation of the Cat Square terrane, southern Appalachian Inner Piedmont, with implications for middle Paleozoic collisional orogenesis. *American Journal of Science*, *317*(2), 95–176. https://doi.org/10.2475/02.2017.01

Janney, P. E., & Castillo, P. R. (2001). Geochemistry of the oldest Atlantic oceanic crust suggests mantle plume involvement in the early history of the central Atlantic Ocean. *Earth and Planetary Science Letters*, *192*(3), 291–302. https://doi.org/10.1016/S0012-821X(01)00452-6

Johnston, J. E., & Christensen, N. I. (1992). Shear wave reflectivity, anisotropies, Poisson's ratios, and densities of a southern Appalachian Paleozoic sedimentary sequence. *Tectonophysics*, *210*(1-2), 1–20. https://doi.org/10.1016/0040-1951(92)90124-O

Kashubin, A. S., & Juhlin, C. (2010). Mapping of crustal scale tectonic boundaries in the Ossa-Morena Zone using reprocessed IBERSEIS reflection seismic data. *Tectonophysics*, *489*(1–4), 139–158. https://doi.org/10.1016/j.tecto.2010.04.010

Keranen, K., & Klemperer, S. L. (2008). Discontinuous and diachronous evolution of the Main Ethiopian Rift: Implications for development of continental rifts. *Earth and Planetary Science Letters*, *265*(1–2), 96–111. https://doi.org/10.1016/j.epsl.2007.09.038

King, S. D., & Anderson, D. L. (1998). Edge-driven convection. *Earth and Planetary Science Letters*, *160*(3-4), 289–296. https://doi.org/10.1016/S0012-821X(98)00089-2

Klitgord, K. D., & Schouten, H. (1986). Plate kinematics of the central Atlantic. In P. R. Vogt, & B. E. Tucholke (Eds.), *The Geology of North America, the Western North Atlantic Region* (Vol. M, pp. 351–378). Geological Society of America. https://doi.org/10.1130/DNAG-GNA-M.351

Liu, M., & Stein, S. (2016). Mid-continental earthquakes: Spatiotemporal occurrences, causes, and hazards. *Earth-Science Reviews*, *162*, 364–386. https://doi.org/10.1016/j.earscirev.2016.09.016

Lizarralde, D., Holbrook, W. S., & Oh, J. (1994). Crustal structure across the Brunswick magnetic anomaly, offshore Georgia, from coincident ocean bottom and multi-channel seismic data. *Journal of Geophysical Research*, *99*(B11), 2,741–21,757. https://doi.org/10.1029/94JB01550

Manatschal, G., Lavier, L., & Chenin, P. (2015). The role of inheritance in structuring hyperextended rift systems: Some considerations based on observations and numerical modeling. *Gondwana Research*, *27*(1), 140–164. https://doi.org/10.1016/j.gr.2014.08.006

Marzoli, A. (1999). Extensive 200-million-year-old continental flood basalts of the Central Atlantic Magmatic Province. *Science*, *284*(5414), 616–618. https://doi.org/10.1126/science.284.5414.616

Marzoli, A., Callegaro, S., Dal Corso, J., Davies, J. H. F. L., Chiaradia, M., Youbi, N., et al. (2018). The Central Atlantic Magmatic Province (CAMP): A review. In L. H. Tanner (Ed.), *The Late Triassic world*, Topics in Geobiology (Vol. *46*, pp. 91–125). Springer International Publishing AG. https://doi.org/10.1007/978-3-319-68009-5_4

Maus, S., Sazonova, T., Hemant, K., Fairhead, J. D., & Ravat, D. (2007). National Geophysical Data Center candidate for the World Digital Magnetic Anomaly Map. *Geochemistry, Geophysics, Geosystems*, *8*, Q06017. https://doi.org/10.1029/2007GC001643

McBride, J. H. (1991). Constraints on the structure and tectonic development of the early Mesozoic South Georgia Rift, Southeastern United States; seismic reflection data processing and interpretation. *Tectonics*, *10*(5), 1065–1083. https://doi.org/10.1029/90TC02682

McBride, J. H., & Nelson, K. D. (1988). Integration of COCORP deep reflection and magnetic anomaly analysis in the southeastern United States: Implications for origin of the Brunswick and East Coast magnetic anomalies. *Geological Society of America Bulletin*, *100*(3), 436–445. https://doi.org/10.1130/0016-7606(1988)100<0436:IOCDRA>2.3.CO;2

McBride, J. H., Nelson, K. D., & Brown, L. D. (1987). Early Mesozoic basin structure and tectonics of the southeastern United States as revealed from COCORP reflection data and the relation to Atlantic rifting. In C. Beaumont, & A. J. Tankard (Eds.), *Sedimentary Basins and Basin-Forming Mechanisms* (pp. 173–184). Calgary, Alta: Canadian Society of Petroleum Geologists.

McBride, J. H., Nelson, K. D., & Brown, L. D. (1989). Evidence and implications of an extensive early Mesozoic rift basin and basalt/diabase sequence beneath the southeast coastal plain. *Geological Society of America Bulletin*, *101*(4), 512–520. https://doi.org/10.1130/0016-7606(1989)101<0512:EAIOAE>2.3.CO;2

McHone, J. G. (2000). Non-plume magmatism and rifting during the opening of the central Atlantic Ocean. *Tectonophysics*, *316*, 287–296.

McHone, J. G. (2003). Volatile emissions from Central Atlantic Magmatic Province basalts: Mass assumptions and environmental consequences. In W. E. Hames, J. G. Mchone, P. Renne, et al. (Eds.), *The Central Atlantic Magmatic Province: Insights from Fragments of Pangea*, *Geophysical Monograph Series* (Vol. 136, pp. 241–254). Washington, DC: American Geophysical Union. https://doi.org/10.1029/136GM013

Merschat, A. J., & Hatcher, R. D. (2007). The Cat Square terrane: Possible Siluro-Devonian remnant ocean basin in the Inner Piedmont, southern Appalachians, USA. In R. D. Hatcher, M. P. J. Carlson, J. H. McBride, & J. R. Martinez Catalan (Eds.), *4-D Framework of Continental Crust*, *Geological Society of America Memoirs* (Vol. 200, pp. 553–565). https://doi.org/10.1130/2007.1200(27)

Milton, C. (1972). Igneous and metamorphic basement rocks of Florida. *Florida Bureau of Geology Bulletin*, *55*, 125.

Morley, C. K. (2010). Stress re-orientation along zones of weak fabrics in rifts: An explanation for pure extension in 'oblique' rift segments? *Earth and Planetary Science Letters*, *297*(3–4), 667–673. https://doi.org/10.1016/j.epsl.2010.07.022

Moser, T. J. (1991). Shortest path calculation of seismic rays. *Geophysics*, *56*(1), 59–67. https://doi.org/10.1190/1.1442958

Mueller, P. A., Heatherington, A. L., Foster, D. A., Thomas, W. A., & Wooden, J. L. (2014). The Suwannee suture: Significance for Gondwana-Laurentia terrane transfer and formation of Pangaea. *Gondwana Research*, *26*(1), 365–373. https://doi.org/10.1016/j.gr.2013.06.018

Nelson, K. D., Arnow, J. A., McBride, J. H., Willemin, J. H., Huang, J., Zheng, L., et al. (1985). New COCORP profiling in the southeastern United States. Part I: Late Paleozoic suture and Mesozoic rift basin. *Geology*, *13*(10), 714–718. https://doi.org/10.1130/0091-7613(1985)13<714:NCPITS>2.0.CO;2

Nelson, K. D., McBride, J. H., Arnow, J. A., Oliver, J. E., Brown, L. D., & Kaufman, S. (1985). New COCORP profiling in the southeastern United States. Part II: Brunswick and east coast magnetic anomalies, opening of the north-central Atlantic Ocean. *Geology*, *13*, 718–721. https://doi.org/10.1130/0091-7613(1982)13<718:NCPITS>2.0.CO;2

Oh, J., Phillips, J. D., Austin, J. A., & Stoffa, P. L. (1991). Deep-penetration seismic reflectionimages across the southeastern United States continental margin. In R. Meissner, L. Brown, H. J. Durbaum, W. Franke, K. Fuchs, & F. Seifert (Eds.), *Continental lithosphere: Deep Seismic Reflections*, *Geodynamics Series* (Vol. 22, pp. 225–240). Washington, DC: American Geophysical Union. https://doi.org/10.1029/GD022p0225

Olsen, P. E., Kent, D. V., Et-Touhami, M., & Puffer, J. (2003). Cyclo-, magneto-, and bio-stratigraphic constraints on the duration of the CAMP event and its relationship to the Triassic-Jurassic boundary. In *The Central Atlantic Magmatic Province: Insights from fragments of Pangea*, *Geophysical Monograph Series* (Vol. 136, pp. 7–32). Washington, DC: American Geophysical Union.

Oyarzun, R., Doblas, M., Lopez-Ruiz, J., & Cebria, J. M. (1997). Opening of the central Atlantic and asymmetric mantle upwelling phenomena: Implications for a long-lived magmatism in western North Africa and Europe. *Geology*, *25*(8), 727. https://doi.org/10.1130/0091-7613(1997)025<0727:OOTCAA>2.3.CO;2

Parker, E. H., Hawman, R. B., Fischer, K. M., & Wagner, L. S. (2013). Crustal evolution across the southern Appalachians: Initial results from the SESAME broadband array. *Geophysical Research Letters*, *40*, 3853–3857. https://doi.org/10.1002/grl.50761

Parker, E. H., Hawman, R. B., Fischer, K. M., & Wagner, L. S. (2015). Constraining lithologic variability along the Alleghanian detachment in the southern Appalachians using passive-source seismology. *Geology*, *43*(5), 431–434. https://doi.org/10.1130/G36517.1

Parker, E. H., Hawman, R. B., Fischer, K. M., & Wagner, L. S. (2016). Estimating crustal thickness using Ss*Pmp* in regions covered by low-velocity sediments: Imaging the Moho beneath the Southeastern Suture of the Appalachian Margin Experiment (SESAME) array, SE Atlantic coastal plain. *Geophysical Research Letters*, *43*, 9627–9635. https://doi.org/10.1002/2016GL070103

Petersen, T. A., Brown, L. D., Cook, F. A., Kaufman, S., & Oliver, J. E. (1984). Structure of the Riddleville Basin from COCORP seismic data and implications for reactivation tectonics. *The Journal of Geology*, *92*(3), 261–271. https://doi.org/10.1086/628859

Pfiffner, O. A. (2017). Thick-skinned and thin-skinned tectonics: A global perspective. *Geosciences*, *7*(3), 71. https://doi.org/10.3390/geosciences7030071

Pickering, S., Higgins, M., & Zietz, I. (1977). Relation between the southeast Georgia embayment and the onshore extent of the Brunswick anomaly. *Eos, Transactions American Geophysical Union*, *58*, 432.

Pollock, J. C., Hibbard, J. P., & van Staal, C. R. (2012). A paleogeographical review of the peri-Gondwanan realm of the Appalachian orogen. *Canadian Journal of Earth Sciences*, *49*(1), 259–288. https://doi.org/10.1139/E11-049

Pratt, T. L., Horton, J. W., Spears, D. B., Gilmer, A. K., & McNamara, D. E. (2015). The 2011 Virginia M_w 5.8 earthquake: Insights from seismic reflection imaging into the influence of older structures on eastern U.S. seismicity. In J. W. J. Horton, M. C. Chapman, & R. A. Green (Eds.), *The 2011 Mineral, Virginia, Earthquake, and its Significance for Seismic Hazards in Eastern North America*, *Geological Society of America Special Paper* (Vol. 509, pp. 285–294). https://doi.org/10.1130/2014.2509(16)

Roland, E., Lizarralde, D., Mcguire, J. J., & Collins, J. A. (2012). Seismic velocity constraints on the material properties that control earthquake behavior at the Quebrada-Discovery-Gofar transform faults. *East Pacific Rise*, *117*(B11), 1–27. https://doi.org/10.1029/2012JB009422

Schlische, R. W. (2003). Progress in understanding the structural geology, basin evolution, and tectonic history of the eastern North American rift system. In P. M. LeTourneau, & P. E. Olsen (Eds.), *The Great Rift Valleys of Pangea in Eastern North America—Volume One: Tectonics, Structure, and Volcanism* (pp. 21–64). New York: Columbia University Press.

Schmandt, B., Lin, F.-C., & Karlstrom, K. E. (2015). Distinct crustal isostasy trends east and west of the Rocky Mountain Front. *Geophysical Research Letters*, *42*, 10,290–10,298. https://doi.org/10.1002/2015GL066593

Schreurs, G., & Colleta, B. (1998). Analogue modelling of faulting in zones of continental transpression and transtension. In R. E. Holdsworth, R. A. Strachan, & J. F. Dewey (Eds.), *Continental Transpressional and Transtensional Tectonics*, (135th ed., Vol. 135, pp. 59–79). London: Geological Society. https://doi.org/10.1144/GSL.SP.1998.135.01.05

Schulte-Pelkum, V., Monsalve, G., Sheehan, A., Pandey, M. R., Sapkota, S., Bilham, R., & Wu, F. (2005). Imaging the Indian subcontinent beneath the Himalaya. *Nature*, *435*(7046), 1222–1225. https://doi.org/10.1038/nature03678

Secor, D. T. J., Samson, S. L., Snoke, A. W., & Palmer, A. R. (1983). Confirmation of the Carolina Slate Belt as an exotic terrane. *Science*, *221*(4611), 649–651. https://doi.org/10.1126/science.221.4611.649

Secor, D. T. J., Snoke, A. W., & Dallmeyer, R. D. (1986). Character of the Alleghanian orogeny in the southern Appalachians: Part III. Regional tectonic relations. *Geological Society of America Bulletin*, *97*(11), 1345–1353. https://doi.org/10.1130/0016-7606(1986)97<1345:COTAOI>2.0.CO;2

Seeber, L., & Armbruster, J. G. (1981). The 1886 Charleston, South Carolina earthquake and the Appalachian detachment. *Journal of Geophysical Research*, *86*(B9), 7874–7894. https://doi.org/10.1029/JB086iB09p07874

Seranne, M., Benedicto, A., Labaum, P., Truffert, C., & Pascal, G. (1995). Structural style and evolution of the Gulf of Lion Oligo-Miocene rifting: Role of the Pyrenean orogeny. *Marine and Petroleum Geology*, *12*(8), 809–820. https://doi.org/10.1016/0264-8172(95)98849-Z

Shervais, J. W., Dennis, A. J., McGee, J. J., & Secor, D. (2003). Deep in the heart of Dixie: Pre-Alleghanian eclogite and HP granulite metamorphism in the Carolina Terrane, South Carolina, USA. *Journal of Metamorphic Geology*, *21*(1), 65–80. https://doi.org/10.1046/j.1525-1314.2003.00416.x

Steltenpohl, M. G., Mueller, P. M., Heatherington, A. L., Hanley, T. B., & Wooden, J. L. (2008). Gondwanan/peri-Gondwanan origin for the Uchee terrane, Alabama and Georgia: Carolina zone or Suwannee terrane(?) and its suture with Grenvillian basement of the Pine Mountain window. *Geosphere*, *4*(1), 131. https://doi.org/10.1130/GES00079.1

Sykes, L. R., Armbruster, J. G., Kim, W.-Y., & Seeber, L. (2008). Observations and tectonic setting of historic and instrumentally located earthquakes in the greater New York City-Philadelphia area. *Bulletin of the Seismological Society of America*, *98*(4), 1696–1719. https://doi.org/10.1785/0120070167

Tauvers, P. R., & Muehlberger, W. R. (1987). Is the Brunswick magnetic anomaly really the Alleghanian suture? *Tectonics*, *6*(3), 331–342. https://doi.org/10.1029/TC006i003p00331

Teyssier, C., Tikoff, B., & Markley, M. (1995). Oblique plate motion and continental tectonics. *Geology*, *23*(5), 447–450. https://doi.org/10.1130/0091-7613(1995)023<0447:OPMACT>2.3.CO;2

Thomas, W. A. (2006). Tectonic inheritance at a continental margin. *GSA Today*, *16*(2). https://doi.org/10.1130/1052-5173(2006)016<4:TIAACM>2.0.CO;2

Tommasi, A., & Vauchez, A. (2001). Continental rifting parallel to ancient collisional belts: An effect of the mechanical anisotropy of the lithospheric mantle. *Earth and Planetary Science Letters*, *185*(1-2), 199–210. https://doi.org/10.1016/S0012-821X(00)00350-2

Trehu, A. M., Ballard, A., Dorman, L. M., Gettrust, J. F., Klitgord, K. D., & Schreiner, A. (1989). Structure of the lower crust beneath the Carolina trough, U.S. Atlantic Continental Margin. *Journal of Geophysical Research*, *94*(B8), 10,585–10,600. https://doi.org/10.1029/JB094iB08p10585

Tull, J. F., Barineau, C. I., Mueller, P. A., & Wooden, J. L. (2007). Volcanic arc emplacement onto the southernmost Appalachian Laurentian shelf: Characteristics and constraints. *Geological Society of America Bulletin*, *119*(3-4), 261–274. https://doi.org/10.1130/B25998.1

van Avendonk, H. J. A., Harding, A. J., Orcutt, J. A., & McClain, J. S. (1998). A two-dimensional tomographic study of the Clipperton fault. *Journal of Geophysical Research*, *103*(B8), 17,885–17,899. https://doi.org/10.1029/98JB00904

van Avendonk, H. J. A., Holbrook, W. S., Lizarralde, D., & Denyer, P. (2011). Structure and serpentinization of the subducting Cocos plate offshore Nicaragua and Costa Rica. *Geochemistry, Geophysics, Geosystems*, *12*, Q06009. https://doi.org/10.1029/2011GC003592

van Avendonk, H. J. A., Holbrook, W. S., Okaya, D., Austin, J. A., Davey, F., & Stern, T. (2004). Continental crust under compression: A seismic refraction study of South Island Geophysical Transect I, South Island, New Zealand. *Journal of Geophysical Research*, *109*, B06302. https://doi.org/10.1029/2003JB002790

Viola, G., Odonne, F., & Mancktelow, N. (2004). Analogue modelling of reverse fault reactivation in strike–slip and transpressive regimes: Application to the Giudicarie fault system, Italian Eastern Alps. *Journal of Structural Geology*, *26*(3), 401–418. https://doi.org/10.1016/j.jsg.2003.08.014

Wagner, L. S., Fischer, K. M., Hawman, R., Hopper, E., & Howell, D. (2018). The relative roles of inheritance and long-term passive margin lithospheric evolution on the modern structure and tectonic activity in the southeastern United States. *Geosphere*, *14*(4), 1385–1410. https://doi.org/10.1130/GES01593.1

West, T. E. J. (1998). Structural analysis of the Carolina-Inner Piedmont terrane boundary: Implications for the age and kinematics of the central Piedmont suture, a terrane boundary that records Paleozoic Laurentia-Gondwana interactions. *Tectonics*, *17*(3), 379–394. https://doi.org/10.1029/98TC01081

Whalen, L., Gazel, E., Vidito, C., Puffer, J., Bizimis, M., Henika, W., & Caddick, M. J. (2015). Supercontinental inheritance and its influence on supercontinental breakup: The Central Atlantic Magmatic Province and the breakup of Pangea. *Geochemistry, Geophysics, Geosystems*, *16*, 3532–3554. https://doi.org/10.1002/2015GC005885

Whitney, J. A., Paris, T. A., Carpenter, R. H., & Hartley, M. E. I. (1978). Volcanic evolution of the southern slate belt of Georgia and South Carolina: A primitive ocean island arc. *The Journal of Geology*, *86*(2), 173–192. https://doi.org/10.1086/649673

Williams, H., & Hatcher, R. D. (1982). Suspect terranes and accretionary history of the Appalachian orogen. *Geology*, *10*(10), 530–536. https://doi.org/10.1130/0091-7613(1982)10<530:STAAHO>2.0.CO;2

Wilson, C. K., Jones, C. H., Molnar, P., Sheehan, A. F., & Boyd, O. S. (2004). Distributed deformation in the lower crust and upper mantle beneath a continental strike-slip fault zone: Marlborough fault system, South Island, New Zealand. *Geology*, *32*(10), 837. https://doi.org/10.1130/G20657.1

Wilson, M. (1997). Thermal evolution of the Central Atlantic passive margins: Continental break-up above a Mesozoic super-plume. *Journal of the Geological Society*, *154*(3), 491–495. https://doi.org/10.1144/gsjgs.154.3.0491

Withjack, M. O., Schlische, R. W., & Olsen, P. E. (2012). Development of the passive margin of eastern North America. In *Regional Geology and Tectonics: Phanerozoic Rift Systems and Sedimentary Basins* (pp. 300–335). New York: Elsevier. https://doi.org/10.1016/B978-0-444-56356-9.00012-2

Wu, Q., Chapman, M. C., & Beale, J. N. (2015). The aftershock sequence of the 2011 Mineral, Virginia, earthquake: Temporal and spatial distribution, focal mechanisms, regional stress, and the role of Coulomb stress transfer. *Bulletin of the Seismological Society of America*, *105*(5), 2521–2537. https://doi.org/10.1785/0120150032

Yuan, X., Sobolev, S. V., Kind, R., Oncken, O., Bock, G., Asch, G., et al. (2000). Subduction and collision processes in the Central Andes constrained by converted seismic phases. *Nature*, *408*(6815), 958–961. https://doi.org/10.1038/35050073

Zelt, C. A., & Smith, R. B. (1992). Seismic traveltime inversion for 2-D crustal velocity structure. *Geophysical Journal International*, *108*(1), 16–34. https://doi.org/10.1111/j.1365-246X.1992.tb00836.x

Zoback, M. L. (1992). First- and second-order patterns of stress in the lithosphere: The World Stress Map Project. *Journal of Geophysical Research*, *97*(B8), 11,703–11,728. https://doi.org/10.1029/92JB00132